KUNGL TEKNISKA HÖGSKOLAN

ISSN 1403-1701 Kärnkraftsäkerhet 6
ISBN 91-7170-496-5
TRITA EKS.Avhandling
ISRN KTH/NPS/MFCI-0005-SE

BREAKUP OF JET AND DROPS DURING PREMIXING PHASE OF FUEL COOLANT INTERACTIONS

Doctoral Thesis

by

Haraldur Óskar Haraldsson

Stockholm
2000

Department of Energy Technology
Division of Nuclear Power Safety
The Royal Institute of Technology
Stockholm, Sweden

Institutionen för Energiteknik
Avd. för Kärnkraftsäkerhet
Kungliga Tekniska Högskolan
Stockholm

Please be aware that all of the Missing Pages in this document were originally blank pages

KUNGL TEKNISKA HÖGSKOLAN

ISSN 1403-1701 Kärnkraftsäkerhet 6
ISBN 91-7170-496-5
TRITA EKS.Avhandling
ISRN KTH/NPS/MFCI-0005-SE

BREAKUP OF JET AND DROPS DURING PREMIXING PHASE OF FUEL COOLANT INTERACTIONS

Doctoral Thesis

by

Haraldur Óskar Haraldsson

May 18, 2000

Royal Institute of Technology

Stockholm, Sweden

KUNGL TEKNISKA HÖGSKOLAN
Royal Institute of Technology
Ecole Royale Polytechnique
Kgl. Technische Hochschule

Postadress:	S-100 44 STOCKHOLM
	Drottning Kristinas väg. 33A
Telephone:	08-790 9254 (National)
	+46 8-790 9254 (International)
Fax:	08-790 9197 (National)
	+46 8-790 9197 (International)
URL:	http://www.egi.kth.se/nps/
Email:	oskar@ne.kth.se

Royal Institute of Technology
100 44 STOCKHOLM
May 2000

Abstract

During the course of a hypothetical severe accident in a light water reactor, molten liquid may be introduced into a volatile coolant, which, under certain conditions, results in explosive interactions. Such fuel-coolant interactions (FCI) are characterised by an initial pre-mixing phase during which the molten liquid, metallic or oxidic in nature, undergoes a breakup (fragmentation) process which significantly increase the area available for melt-coolant contact, and thus energy transfer. Although substantial progress in the understanding of phenomenology of the FCI events has been achieved in recent years, there remain uncertainties in describing the primary and secondary breakup processes.

The focus of this work is on the melt jet and drop breakup during the premixing phase of FCI. The objectives are to gain insight into the premixing phase of the FCI phenomena, to determine what fraction of the melt fragments and determine the size distribution. The approach is to perform experiments with various simulant materials, at different scales, different conditions and with variation of controlling parameters affecting jet and drop breakup processes. The analysis approach is to investigate processes at different level of detail and complexity to understand the physics, to rationalise experimental results and to develop and validate models.

In the first chapter a brief introduction and review of the status of the FCI phenomena is performed. A review of previous and current experimental projects is performed. The status of the experimental projects and major findings are outlined.

The first part of the second chapter deals with experimental investigation of jet breakup. Two series of experiments were performed with low and high temperature jets. The low temperature experiments employed cerrobend-70 as

jet liquid. A systematic investigation of thermal hydraulic conditions and melt physical properties on the jet fragmentation and particle debris characteristics was performed. The coolant temperature was found to significantly affect the shape and size of the debris. The maximum fragment size was found to increase with reduction in coolant temperature. No effect of coolant voiding on the fragment size distribution was observed. A series of high temperature melt jet experiments were performed, in the MIRA-20L experimental facility. Three types of oxidic melts, namely; CaO-B_2O_3, MnO-TiO_2 and WO_3-CaO were employed as melt jet liquid. The melt jet fragmentation was classified into two regimes, the hydrodynamic-controlled regime and the solidification-controlled regime. The delineation between those regimes was observed from the size characteristic and morphology of the solidified debris which was formed. The temperature of the coolant was the primary parameter in determining which regime the jet fragmentation would fall into. It was found, at low subcooling, the fragments are relatively large and irregular compared to smaller particles produced at higher subcooling. The melt density was found to have significant effect on the particle size. The mass mean size of the debris changes proportional to the square root of the coolant to melt density ratio. A systematic investigation of the performance of statistical distributions which may be used to describe the size distributions of fragments obtained from molten fuel coolant interaction (MFCI) experiments was performed. The statistical analysis of the debris produced in both experiments showed that the sequential fragmentation theory fits best the particle distribution produced during the jet fragmentation process.
In the second part of the second chapter, analysis of the jet breakup experiments are performed. The low temperature jet fragmentation experiments are simulated with a recently developed Multiphase Eulerian Lagrangian Method (MELT-3D). The effect of particle diameter and particle drag on the jet dynamics and penetration behavior is investigated.
The third part of the second chapter deals with simulation of Kelvin-Helmholtz instabilities. A high order Navier-Stokes solver is employed along with the front tracking Level-Set algorithm, to eliminate numerical diffusion. The effect of surface tension and viscosity on the development of instabilities is investigated. Three regimes are identified, and delineated, based on Weber and Ohnesorge numbers.

The third chapter is devoted to brekup of liquid drops in water. The emphasis is directed towards delineating the roles which melt to coolant heat transfer, melt solidification, melt fusion heat and melt mushy zone play in the fragmen-

tation process. Coolant temperature is found to have a significant impact on the droplet fragmentation behaviour for subcooled conditions. The melt superheat greatly affects the characteristic time for solidification, and thus strongly affects the deepness of the fragmentation process. The fusion heat of the eutectic melt contributes significantly to the solidification time scale, and thereby enables the eutectic melt drop to feature deeper fragmentation. The presence of the mushy zone during the phase change of the non-eutectic melts significantly prevents these melt drops from completing the deformation and fragmentation process, especially when the melt superheat is small. An instability analysis on the crust breakup was performed. A modified dimensionless Aeroelastic number Ae_* is obtained as a criteria for breakup of the plain crust. It is found that the modified Aeroelastic number can be employed to evaluate the breakup behaviour of a droplet with a thin solidified layer on its surface.

Keywords: *light water reactor, severe accident, melt-structure-coolant interactions, heat transfer, jet breakup, drop breakup, multiphase flow, multiphase interactions, instabilities, phase change, mushy zone.*

Preface

Research results, presented in the present thesis, were obtained by the author during the period between 1997 and 2000. The work was performed at the Nuclear Power Safety Division of Royal Institute of Technology (KTH). The results of these research activities have been summarized and described in the following publications:

1. **H.Ó. Haraldsson**, H.X. Li, T.N. Dinh, J.A. Green and B.R. Sehgal, "Hydrodynamic Fragmentation of a Molten Metal Jet in Water: Effect of Melt Solidification and Coolant Voiding", Twelfth Proceedings of Nuclear Thermal Hydraulics, American Nuclear Society (ANS), 1997, pp. 125-134.

2. **H.Ó. Haraldsson** and B.R. Sehgal, "Particle Size Distribution in Molten Fuel-Coolant Interactions and Parameters of the Sequential Fragmentation Theory", Proceedings of the Third International Conference on Multiphase Flow 98, (ICMF98), June 8-12, 1998, Lyon, France.

3. H.X. Li, **H.Ó. Haraldsson**, T.N. Dinh, J.A. Green and B.R. Sehgal, "Fragmentation Behaviour of Melt Drop in Coolant: Effect of Melt Solidification", Proceedings of the Third International Conference on Multiphase Flow 98, (ICMF98), June 8-12, 1998, Lyon, France.

4. H.X. Li , T.N. Dinh, **H.Ó. Haraldsson** and B.R. Sehgal, "Fragmentation Behavior of Melt Drops in Coolant: Effects of Melt Fusion Heat and Mushy Zone", 4th International Symposium on Multiphase Flow and Heat Transfer, August 22-24, 1999, Xi'an, China, pp 511-518.

5. **H.Ó. Haraldsson** and B.R. Sehgal, "Effect of Subcooled Liquid Coolant on Particle Size Generated During Fuel Coolant Interactions", 37th European Two-Phase Flow Meeting, September 28 - 30, 1999, London, England.

6. **H.Ó. Haraldsson** and B.R. Sehgal, "Breakup of High Temperature Oxide Jet in Water", Ninth International Topical Meeting on Nuclear Rreactor Thermal Hydraulics (NURETH-9), October 3 - 8, 1999, San Fransisco, USA.

7. **H.Ó. Haraldsson** and B.R. Sehgal, "Characterization of Debris Bed Generated by Fuel Coolant Interactions", OECD Workshop on Ex-Vessel Debris Coolability, November 16 - 18, 1999, Karlsruhe, Germany.

8. **H.Ó. Haraldsson**, H.X. Li, Z.L. Yang, T.N. Dinh and B.R. Sehgal, "Effect of Solidification on Drop Fragmentation in Liquid-Liquid Media", Research Journal of Heat and Mass Transfer. (submitted)

9. **H.Ó. Haraldsson**, R.R. Nourgaliev, T.N. Dinh, and B.R. Sehgal, Investigation of Melt Jet Fragmentation in Water: Effects of Thermophysical Properties and Melt Solidification", International Journal of Thermal Science. (submitted)

10. H.X. Li, **H.Ó. Haraldsson**, T.N. Dinh and B.R. Sehgal, "Fragmentation Behaviour of Melt Drop in Coolant", International Journal of Thermal Science. (submitted)

11. **H.Ó. Haraldsson**, I.V. Kazachkov, T.N. Dinh and B.R. Sehgal, "Analysis of Thin Jet Breakup Length in Immiscible Fluids", Third International Conference on Advances in Fluid Mechanics, Montreal, Canada, May 24-26, 2000.

12. A.T. Dinh, **H.Ó. Haraldsson**, Z.L. Yang and B.R. Sehgal, "Simulation of Viscous Stabilization of Kelvin-Helmholtz Instabillities", Third International Conference on Advances in Fluid Mechanics, Montreal, Canada, May 24-26, 2000.

13. R.R. Nourgaliev, T.N. Dinh, A.T. Dinh, **H.Ó. Haraldsson** and B.R. Sehgal, "The Multiphase Eulerian-Lagrangian Transport (MELT-3D) Approach for Modeling of Multiphase Mixing in Fragmentation Processes", International Journal of Multiphase Flow. (submitted)

14. A.T. Dinh, **H.Ó. Haraldsson**, Z.L. Yang, T.N. Dinh and B.R. Sehgal, "A Numerical Study of Kelvin-Helmholtz Instabillities by the Level-Set Approach", ASME Fluids Engineering Summer Conference, Boston, USA, June 11-15, 2000.

15. **H. Ó. Haraldsson** and B.R. Sehgal, "Effect of Crust Formation on Drop Breakup Behaviour", National Heat Transfer Conference, Pittsburg, USA, August 20-22, 2000.

16. B.R Sehgal, Z.L. Yang, T.N. Dinh, R.R. Nourgaliev, V.A. Bui, **H. Ó. Haraldsson**, H.X. Li, M. Konovalikhin, D. Paladino and W.H. Leung "Investigation on Melt-Structure-Water Interactions (MSWI) during Severe Accidents", SKI report 99:42, 1999, (ISSN 1104-1374).

17. B.R Sehgal, Z.L. Yang, **H.Ó. Haraldsson**, R.R. Nourgaliev, M. Konovalikhin, D. Paladino, A.A. Gubaidullin, G. Kolb and A. Theerthan "Phenomenological Studies on Melt-Structure-Water Interactions (MSWI) during Severe Accidents", SKI report. (report)

18. **H.Ó. Haraldsson**, Z.L. Yang and B.R. Sehgal, "Analytical Study of Single Droplet Fragmentation in Liquid Coolant", 5th International Symposium on Heat Transfer, August 12-16, 2000. Beijing, China.

19. I. Kazachkov, Z.L. Yang, **H.Ó. Haraldsson** and B.R. Sehgal,"Instability analysis of thin film flow dynamics in a micro-channel", 5th International Symposium on Heat Transfer, August 12-16, 2000. Beijing, China.

Contents

List of Figures

List of Tables

Nomenclature

Arabic

Ae	Aeroelastic number
C	Heat capacity, constant
D	Bending stiffness, jet diameter
D_f	Fractal dimension
d_o	Initial drop or jet diameter
E	Elasticity modulus or Young's modulus
e	Error
Fr	Froude number
f	Drag enhanchement factor
g	Acceleration
H_{fus}	Heat of fusion
h_{fg}	Enthalpy of Vaporization
i	Imaginary unit
k	Wave number = $2\pi/\lambda$
m	Instability mode
N	Number of fragments
n	Wave growth
Oh	Ohnesorge number
p	Pressure, fitted numbers
P_i	Pressure in fluid i
Pr	Prandtl number
q	Heat
q"	Heat flux
R	Radius
Re	Reynolds number
r	Fractional size
Sm	Structural merit number
s	Standard deviation

T_i	Temperature of fluid i
t	time
U_i	Velocity of fluid i
$\mathbf{u}$	Velocity (U,V,W)
u	velocity in x direction
v	velocity in y direction
We	Weber number

Greek

α	Density ratio, wave number
β	Viscosity ratio, perturbation growth rate
δ	Crust thickness, surface disturbance
ϕ	Velocity potential
η	Surface displacement
ϵ	Poissons ratio
γ	Fractal parameter
κ	Thermal conductivity
λ	Wavelength
μ	Dynamic viscosity
ν	Kinematic viscosity
σ	Surface tension
ρ_i	Density of fluid i
τ_f	Characteristic time
φ	Void fraction
ω	Wavelength

Subscripts/Superscripts

1	Drop
2	Ambient
a	Ambient
c	Critical, coolant
d	Drop
$frag$	Fragmentation
fus	Fusion
$hydr$	Hydrodynamic
ini	Initial
j	Jet
l	Liquid
MMS	Mass Mean Size
o	Initial

sol	Solidification
sup	Superheat
v	Vapour

List of acronyms

ABB	Asea Brown Boveri
BWR	Boiling Water Reactor
FCI	Fuel - Coolant Interaction
LWR	Light Water Reactor
MFBT	Minimum Film Boiling Temperature
MFCI	Molten Fuel - Coolant Interaction
SFT	Sequential Fragmentation Theory
LN	Log Normal Distribution
ULLN	Upper Limit Log Normal Distribution

Acknowledgements

First of all I would like to thank my supervisor Professor B.R. Sehgal for providing excellent support and guidance during my graduate studies. A lot of thanks go to my advisor Adj. Associate Professor T.N. Dinh (Nam), for his endless help, stimulation and discussion during my studies. His advise really helped me to find my track towards the subject. Valuable comments and discussions with my collegue and office mate Dr. Z.L. Yang (Lin) is greatly acknowledge, he kept on challenging me after Nam moved overseas. I feel lucky to have cooperated with Dr. H.X. Li (Li), Adj. Assistant Professor R.R. Nourgaliev (Robert), Dr. I.V. Kazachkov (Ivan) and Mr. A.T. Dinh (Tuan) on scientific subjects related to MFCI. Other collegues and friends at the NPS/RIT division, thank you guys for being here with me during this period of time.

I want to express my gratitude to my collegues at the Thermal/Fluids Laboratory at the Department of Mechanical Engineering of the University of Icleand: Professor and Dean of Engineering V.K. Jónsson, Associate Professor Ó.P. Pálsson, Professor G.R. Jónsson and Professor P. Valdimarsson for their support throughout my earlier studies.

Finally, I would like to thank my wife Gudrún and my daughter Erla for their love, support and patience during the last three years.

The work performed in this thesis was financially supported, in the frame of the following projects:

1. *"Experiments on Melt-Structure-Water Interactions during Severe Accidents"* funded by Swedish Nuclear Power Inspectorate (SKI), Swedish Power Companies Vattenfall, Sydkraft, Forsmark, Finnish Power Company TVO under the auspice of the APRI project;
2. *"Experiments on Melt-Structure-Water Interactions during Severe Accidents"* funded by Finnish Power Companies IVO and TVO and the Finnish National Laboratory VTT;

3. *"Experiments on Melt-Structure-Water Interactions during Severe Accidents"* funded by Swiss Nuclear Power Safety Inspectorate (HSK);

4. *"Experiments on Melt-Structure-Water Interactions during Severe Accidents"* funded by the Nordic joint Nuclear Safety Project NKS;

5. *"Molten Fuel-Coolant Interactions MFCI"* Project funded by European Union (Fourth Framework Programme).

I would like to thank all of my sponsors for the financial support provided and to their representatives Mr. V. Gustavsson, Mr. R. Espefal, Mr. H. Dubik, Dr. W. Frid, Dr. Ninos Garis, Dr. S. Basu, Dr. H. Tuomisto and Dr. A. Zurita who provided review of the work performed in this thesis.

Summary of Technical Accomplishments and Contributions

	Technical Accomplishments and Contributions	*Chapters Appendices*
	I. Breakup of Liquid Jet	
1	Experiments were conducted to investigate the impact of thermal-hydraulic conditions upon the fragmentation behavior and particle debris bed characterization for the interaction of a melt jet in water. An alloy with 70°C melting point was used as jet liquid in non-boiling mode experiments where coolant conditions were varied to provide insight into jet fragmentation with and without melt freezing. Coolant temperature is found to significantly affect both the size and the shape of particles stripped/ fragmented from the melt jet. Coolant tank void fractions (air) up to 20% did not reveal any substantial impact on the average particle size or size distribution.	Chapter 2, App.A

	Technical Accomplishments and Contributions	*Chapters Appendices*
I. Breakup of Liquid Jet (cont.)		
2	A series of 22 experiments employing three high melting point binary oxides, CaO-B_2O_3, MnO_2-TiO_2 and WO_3-CaO were performed. The coolant temperature was found to significantly affect the shape, size, size distribution and porosity of the particle bed produced. For higher coolant subcooling smaller particles are produced compared to those for low subcooling. The mass mean size of the particles produced was found to decrease with the root of the melt to coolant density ratio.	Chapter 2, App.B
3	A comparison of four statistical distributions, namely: Weibull, log-normal and upper limit log-normal distributions along with the distribution resulting from the sequential fragmentation theory (SFT) to describe the size distributions of fragments obtained from molten fuel coolant interactions (MFCI) experiments, is performed. It is found, among the distributions examined, that the SFT model, using mass mean diameter σ and a free parameter γ, which represent the fractal dimension of the debris, describe the measured data better than the other distributions.	Chapter 2, App.A, App.C
4	The MELT-3D method is employed to investigate fragmentation of melt jet in coolant. It is found that the model is capable of describing the evolution of the melt-coolant multiphase mixing process with reasonable accuracy. Effects of variations in jet/coolant velocities, and of coolant thermophysical properties are analyzed, with particular emphasis on their implications for the fragmentation and mixing processes.	Chapter 2, App.D

	Technical Accomplishments and Contributions	*Chapters Appendices*
I. Breakup of Liquid Jet (cont.)		
5	Development of Kelvin-Helmholtz instability on a horizontal surface was investigated numerically. The numerical method combines the advanced Level-Set Algorithm (LSA) for interface tracking with the high order Variable Density (VarDen) method for solution of the Navier-Stokes equations. The effect of surface tension and viscosity on the evolution of Kelvin-Helmholtz instabillities are discussed and three different regimes, depending on Weber and Reynolds numbers, are defined.	Chapter 3, App.E
II. Fragmentation of Drops		
6	Experimental investigation of melt droplet fragmentation using Pb-Bi alloys at both eutectic and non-eutectic compositions was performed. Coolant temperature is found to have a significant impact on the droplet fragmentation behaviour for subcooled conditions. Typically, the droplet fragmentation can be roughly categorised in two regimes: the fragmentation-controlled regime, and the freezing-controlled regime. The solidification and the fragmentation processes and their time scales compete with each other.The fusion heat of the eutectic melt contributes significantly to the solidification time scale, and thereby enables the eutectic melt drop to feature deeper fragmentation.	Chapter 3, App.F

	Technical Accomplishments and Contributions	*Chapters Appendices*
II. Breakup of Drop (cont.)		
7	The presence of the mushy zone during the phase change of the non-eutectic melts significantly prevents these melt drops from completing the deformation and fragmentation process, especially when the melt superheat is small	Chapter 3, App.F
8	A linear stability analysis of the interface between the two liquid fluids with thin crust growing between them, is performed. A modified dimensionless Aeroelastic number, for Kelvin-Helmholtz instability, is obtained and used as a criterion for fragmentation of molten drops penetrating into another liquid coolant medium with lower temperature. The nondimensionalized mean diameter of the fragmented particles is correlated with the Aeroelastic number.	Chapter 3, App.G

Chapter 1

Introduction

The introduction of a hot, molten liquid into a volatile coolant can, under certain conditions, result in explosive interactions. Such fuel-coolant interactions (FCI) are characterized by an initial premixing phase during which the molten liquid, metallic or oxidic in nature, undergoes a fragmentation process which significantly increase the area available for melt-coolant contact, and thus energy transfer. Although substantial progress in the understanding of phenomenology of the FCI events has been achieved in recent years, there remain uncertainties in describing the breakup (fragmentation) processes. The scale of interest can vary from a single droplet up to a large diameter, high temperature, jet falling into water. Such fuel-coolant interactions are of interest to the nuclear, chemical, metal, glass and paper industries as well as to the study of volcanic eruption. Of particular relevance to this work are those situations, during a hypothetical severe accident in a light water nuclear reactor power plant, in which molten oxidic-metallic melts at temperatures in excess of 2800 K interact with water either inside, or outside the reactor pressure vessel.

1.1 Fuel Coolant Interaction (FCI)

Severe accidents in a light water reactor could lead to fuel-coolant interactions (FCIs) during the pouring of molten core material into a water pool. Such a mode of contact, which could occur *in-vessel* or *ex-vessel*, see figure 1.1, would result in vigorous thermal interactions, intense steam generation and, potentially, steam explosions. The thermal processes, in their turn, largely depend on hydrodynamic behaviour, such as

core melt jet breakup, droplet fragmentation, stability of vapor film, all of which can be characterized as surface (interface) instability phenomena.

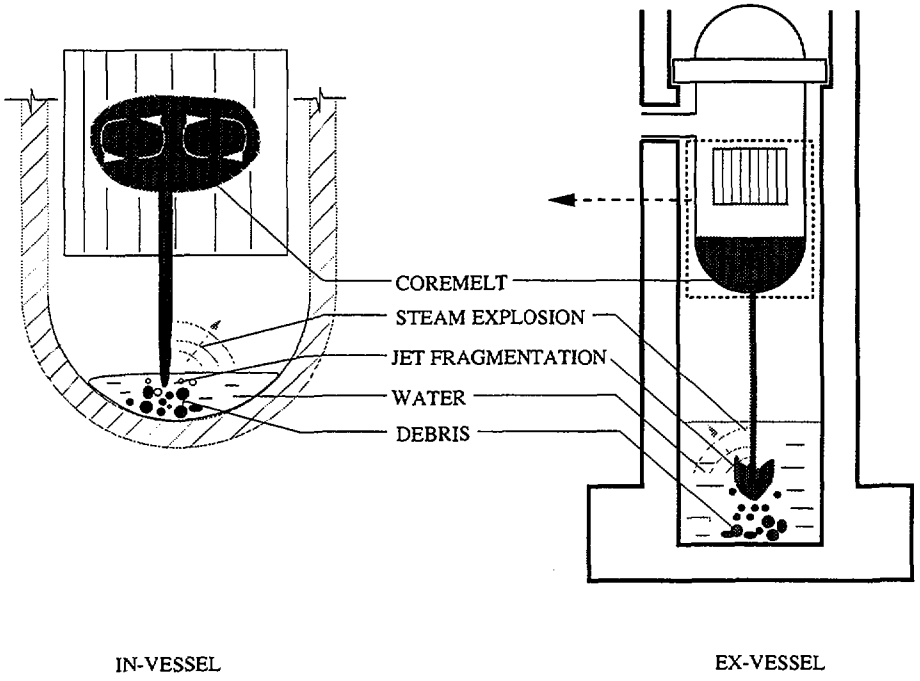

Figure 1.1: Schematic of in-vessel and ex-vessel FCI

1.1.1 The FCI process

In general the FCI process can be roughly divided into four phases [16] [79]; (i) the initial coarse mixing phase or premixing (ii) the trigger phase (iii) the detonation propagation phase and (iv) the hydrodynamic expansion phase.

The initial premixing phase is characterized by the entry of molten fuel material into the water coolant. The fuel enters in the form of jets or drops which interact with the water, with accompanying mixing of melt material, water and vapor generation. The melt jets and drops break up into smaller diameter drops. The breakup process is mainly governed by two types of hydrodynamic instabilities, namely; the Rayleigh-Taylor and Kelvin-Helmholtz instabilities. The breakup process is either driven by the melt decceleration or by the velocity difference between the melt and the coolant surrounding it. The vapor film around the molten fuel insulates it from the water. This prevents cooling of the fuel particles and thus lowers their cooling rate.

The process enters the triggering phase when the vapor film, around the molten fuel, collapses due to some disturbances. The collapse of the vapor film allows the water to come in near contact, or in contact, with the molten fuel which enhances the heat transfer between the molten fuel and the surrounding water and increases the velocity in the vicinity of the trigger. If the triggering event is energetic enough the MFCI process enters the next phase, the detonation propagation phase.

The detonation propagation phase is characterized by the sharp micro interaction zone which propagates through the entire mixing zone. In the micro interaction zone the molten fuel is fragmented to small particles, resulting in rapid increase in interfacial area between the fuel and coolant. This increases the transfer of heat to the surrounding water and generation of shock waves. The same instabilities as in the premixing phase could be responsible for the rapid fine fragmentation of the molten fuel during the detonation propagation phase.

In the expansion phase the thermal energy is converted into mechanical energy which acts on the surrounding.

Each stage of the process involves considerable phenomenological uncertainties and further efforts are required in order to reduce the uncertainties in predicting steam explosion energetics. The current thesis focuses on the initiation of the premixing phase of the fuel coolant interactions, i.e. the melt jet and droplet breakup processes.

1.1.2 The in-vessel and ex-vessel scenarios

The in-vessel FCIs are of great importance from two points of view. First, the energetics and destructive forces of a potential in-vessel steam explosion (α - mode) could present a potential threat to the vessel and integrity of the surrounding containment. Recent studies, see e.g. Theofanous and Yuen [68], Speis and Basu [65] and Turland et.al. [72] on in-vessel FCI have led to the conclusion that containment failure due to the potential steam explosion is highly unlikely or may be impossible. This conclusion has reduced the significance of the in-vessel steam explosion. Secondly, fragmentation behaviour and interface area evolution of the fragmented core melt determines the configuration of the debris bed formed in the lower plenum of the reactor pressure vessel. Furthermore, if the molten corium jet breaks up during its interaction with the water, it does not impinge on the vessel wall and hence ablate the vessel wall.

The ex-vessel scenario FCIs is more important. Such a hypothetical situation may arise in the newer ABB boiling water reactor (BWR) plants which are located in Sweden and Finland. These plants employ a severe accident management procedure, in

which a deep, highly-subcooled, water pool is established under the vessel, as soon as it becomes clear that the water level in the core may fall below the top of the fuel. The motivation for this strategy is the engineering judgement that the core melt jet will break up during its passage through the water and that the debris bed formed can be cooled permanently within the water pool. The success of this procedure is predicated upon the judgement that a large steam explosion, which could threaten the containment integrity during the melt-water interaction, will not occur.

1.2 Molten Fuel-Coolant Premixing

1.2.1 Status of current research and recent results

Currently, several large-scale experimental programs and analyses efforts are underway to determine physical mechanisms associated with FCIs and to provide models and methods, which could be used to predict the consequences of FCIs in reactor accident situations; see e.g. recent reviews by Turland and Dobson [71], Berthoud [5], Magallon et al. [47]. Although remarkable progress in the description of the pre-mixing and expansion phases of the steam explosion has been achieved in recent years, the initial part of the premixing phase has not been well understood yet. This includes jet break up, droplet formation and subsequent fragmentation.

Analytical studies on jet instability have been pursued, lately, at IKE (Stuttgart, Germany) by Bürger and co-workers [11], and at CENG (Grenoble, France) by Berthoud and co-workers [5]. During this period, several experimental programs have also been pursued. Specifically, the MIXA [16], MAGICO [2], BILLEAU [6], and QUEOS [52] tests were conducted, employing jet-like configurations of hot spheres, to obtain data for validation of the pre-mixing models in FCI codes see e.g. Thefanous et al. [69] and Berthoud [5]. The interactions of prototypic melt material with water were experimentally investigated in FARO and KROTOS (Ispra, Italy) [50], [49]. The PREMIX (FzK, Karlsruhe, Germany) [47] tests employed molten Al_2-O_3 at high temperature. The JEFRI tests (IKE, Stuttgart, Germany) [11] at low temperatures, employed Wood's metal as jet simulant fluid and freon R113 as coolant. In the high-temperature tests the melt mass was limited, so that a quasi-steady process was not achieved.

In the FARO facility, large masses (typically, up to 250 kg) of prototypic reactor melt are generated and poured into a water pool of varying depths at a range of system pressures. The FARO tests performed so far, melt cooling with no steam explosion. The tests suggest that erosion of the jet column is an efficient contributor to break-up

throughout the melt fall in water. They showed that significant amount of hydrogen were produced during quenching of a pure oxidic melt (e.g., 0.32 kg in L-24). Possible hydrogen blanketing of melt may also explain the difficulty experienced in triggering an explosion in the KROTOS experiments with prototypic melt.

For BWR plants, there exists a large amount of metal melt which may be discharged to the drywell water pool in form of jets. It was also postulated that the prototypic melt with a metallic component may be more conducive to triggering. On the other hand, it has also been postulated that hydrogen may play a role in suppressing augmentation. The experimental program at the Argonne National Laboratory has focused on whether chemical augmentation of the energetics can occur in Zr-water and Zr-ZrO_2-water steam explosion. Melt quantities up to 1 kg of both Zr-water and Zr-ZrO_2-water were dropped into a column of subcooled water. Explosions took place only when an external trigger was used. In the triggered tests, the extent of oxidation of zirconium melt was very extensive. However, the explosion energetics estimated were very small compared to the potential chemical energy available from the oxidation reaction. This indicates limited chemical augmentation during the explosion time scale.

In the PREMIX experimental program, 14 tests were conducted to date. Up to 20 kg of Al_2O_3 at 2600 K was poured into saturated or subcooled water. In the tests PM10 and PM11, the water depth was small (0.5 m) while the jet diameter was 57 mm (in PM10) and 3x32 mm (in PM11). Only part of the melt was fragmented and solidified. One mild steam explosion occurred in the triple-nozzle test PM11 with saturated water after the melt was settled on the test-section bottom and the quasi-steady boiling was established. Likely, the stratified explosion was triggered when water came into contact with the melt after collapse of the jet-induced vapor chimney. The energetics and the conversion ratio were small. The PM12 to PM14 test were conducted to study the reproducibility of results under nominally identical starting conditions. No conditions were found under which a steam explosion was expected.

1.2.2 Inter-relations and uncertainties of molten fuel-coolant premixing

A large number of heat and mass transfer phenomena occur during MFCIs. Phenomenological uncertainties associated with melt-water interactions are contributed by the complex nature of, and feedbacks between, melt-water hydrodynamic and thermal interactions. The schematic representation of these interactions, and feedbacks is shown in Fig.1.2.

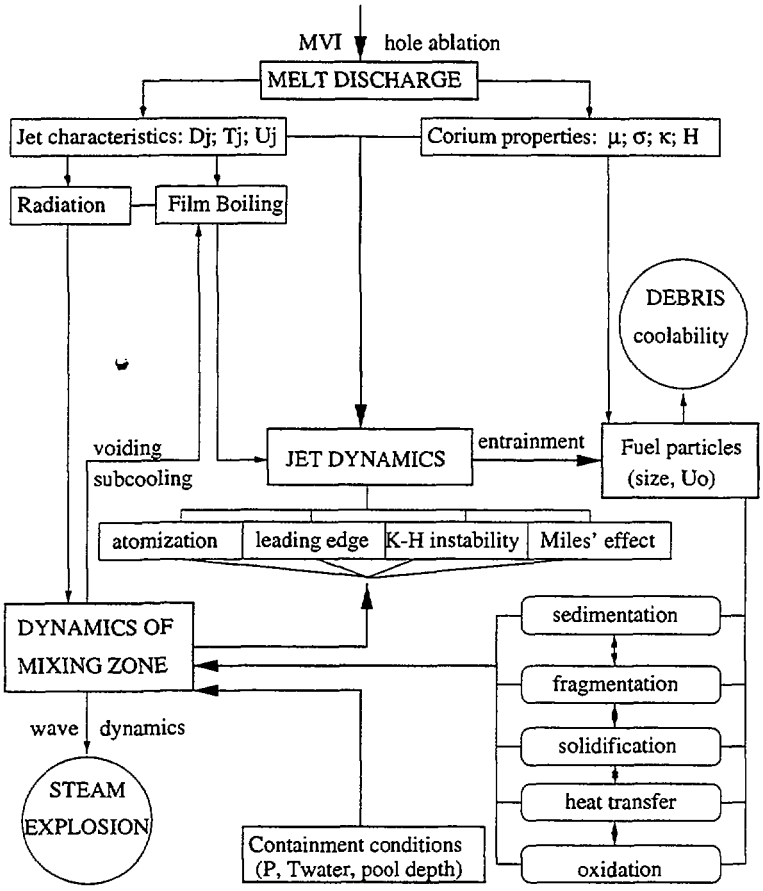

Figure 1.2: Major phenomena and inter-relations under melt jet fragmentation and melt-coolant mixing (D_j, T_j, U are jet diameter, temperature and velocity; μ, σ, κ, H are the melt viscosity, surface tension, conductivity and latent-heat-of-fusion).

In the premixing phase, the fragmentation behaviour of the core melt is governed by various instability mechanisms, developed as a result of (liquid-liquid) contact and relative movement between corium and coolant. Fragmentation of narrow melt jets, for instance, is governed by the capillary instability, brought about by surface tension effects at low velocities. Fragmentation of larger jets is driven by two major mechanisms, termed as *Rayleigh-Taylor* and *Kelvin-Helmholtz* instabilities. At the head of the jet, Rayleigh-Taylor instability is likely to occur, when the jet penetration is resisted by the stagnation pressure arising from the ambient fluid, which has to be displaced. As the flow velocity into the head is likely to be greater than the velocity of the head moving down, the flow of jet material must spread sideways, even being swept back by the upflow of the ambient liquid. Development of unstable perturbations at the leading edge

could lead to break-up of the head structure. Away from the jet head, Kelvin-Helmholtz instabilities (instabilities that occur when there is strong shear in the velocity profiles, between the fluid in the jet and the ambient liquid outside) may occur on the body of the jet. Such type of instability leads to oscillations of the jet surface, which may develop and cause stripping of jet material from the jet (jet erosion or jet atomization) and a droplet field would develop. Corium drops or particles might further fragment in the flow field due to the same instability mechanisms, which govern jet fragmentation. Sequential fragmentation of the melt drops would lead to the formation of very fine debris structure.

Thermal interactions between core melt and water are governed by the heat transfer from the melt to water by film boiling and heat radiation. Under the thermal exchange the melt would cool down and solidify, while the water would heat up and vaporise. The change of melt properties during its solidification, as well as the formation of a two-phase (water-steam) zone around the melt field, would significantly affect further melt fragmentation and mixing.

Parameters of importance are also specified in Fig.1.2. Complex feedbacks and the lack of appropriate database at high temperatures are the major obstacles to development of mechanistic models of MFCIs.

The key scenario uncertainties for ex-vessel melt-coolant premixing can be categorized into two groups.

1. Water pool conditions, which can vary depending on the water available, the geometrical characteristics of the drywell, and the accident management actions undertaken.
2. Melt conditions. The mode and length scale (diameter) of melt discharge, the melt superheat and composition, the number of simultaneous jets, etc. largely depend on in-vessel melt progression scenarios, and the mode of vessel failure.

1.2.3 Self-limiting mechanisms in melt-water premixing

Recently, in the FARO core melt quenching experiments, it was observed that a system equilibrium appears to exist in the long-poure jet scenarios. Feedback between jet fragmentation and mixing-zone voiding was articulated as being responsible for the self-limiting mechanism observed (Fig.1.3).

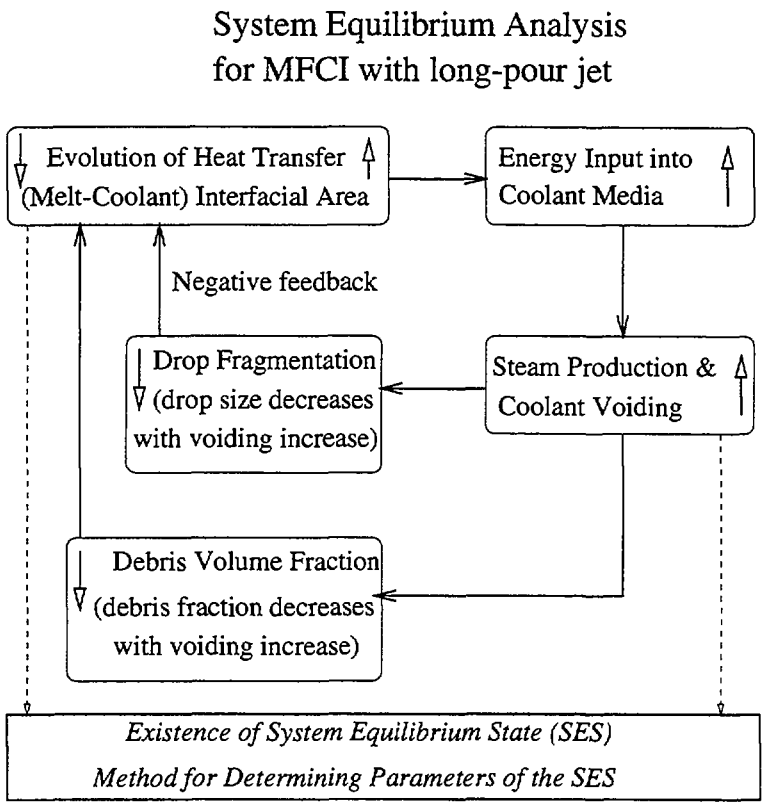

Figure 1.3: Feedback relations and system equilibrium.

This observation and argument indicate that, for given melt and coolant conditions and properties, the system tends to reach its equilibrium state shortly. This particularly justifies the use of quasi-steady state modeling of jet-coolant premixing in the present assessment.

Furthermore, some characteristics of melt jet-coolant premixing appear to have a favourable impact on the steam explosion energetics. It has been observed from simulant material test that at higher subcoolings there may be a greater potential for vapor film collapse, and hence triggering. Thus, triggerability is, likely, greater in the initial period of melt relocation to subcooled water pool. The energetics of steam explosions is however limited in the early phase of melt-coolant premixing, since the amount of melt in the premixing zone is limited while water in the interaction zone is highly subcooled. The initial premixing will also occur near the coolant surface facilitating explosion venting. Therefore, it is expected that the increased triggerability in the initial mixing period is coupled with the decreased energetics due to the melt mass limitation and explosion venting (see Fig.1.4).

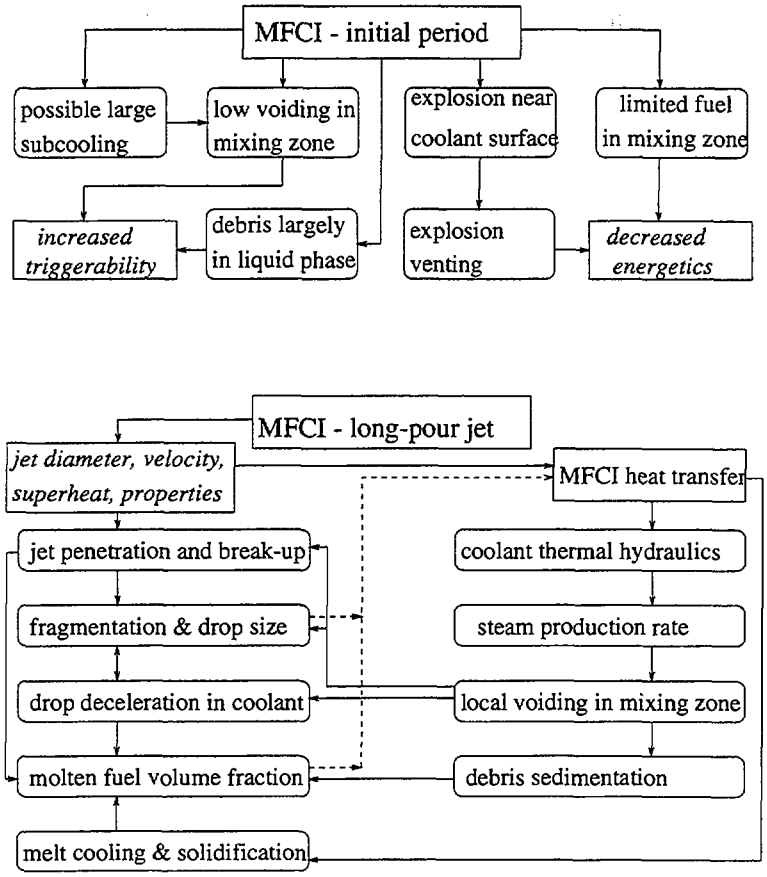

Figure 1.4: Phenomenological relations in initial period and steady configuration of jet-coolant premixing.

1.3 Present Work

The present work aims to investigate the molten jet and drop-coolant interactions, with particular emphasis on the physical mechanisms which may govern instability and fragmentation of a jet or a drop penetrating into a vaporizing coolant pool.

The present thesis consists of two parts. The first part deals with breakup of liquid jet under FCI conditions. An experimental investigation of jet breakup at low and high temperatures was performed and the effect of different flow and physical parameters, i.e. jet density, coolant temperature, jet temperature etc. were observed. A multiphase Eulerian-Lagrangian particle tracking method (MELT-3D) was employed to simulate the jet breakup process and to investigate the effect of different physical parameters on

the jet breakup. The effect of surface tension and viscosity on development of Kelvin-Helmholtz instability on a horizontal surface was investigated numerically. The numerical method combines the advanced Level-Set Algorithm (LSA) for interface tracking with the high order Variable Density (VarDen) method for solution of the Navier-Stokes equations.

The second part of the thesis is focused on the breakup of drops. The effect of coolant temperature and melt superheat, i.e. of heat transfer on the breakup process is investigated. Furthermore the effect of melt fusion heat and melt mushy zone is determined. A linear analysis of Kelvin-Helmholtz instability with crust formation is developed. A dimensionless number, the modified Aeroelastic number (Ae) is obtained and established as a criterion for the breakup of the drops.

Chapter 2

Breakup of Liquid Jet under FCI conditions

2.1 Introduction

Instability and breakup of a liquid jet penetrating into another fluid has attracted the attention of numerous investigators. A pioneering study in this field was performed by Platau (1873) [61] and Rayleigh (1879) [62]. Platau observed, based on surface energy, that uniform circular cylindrical jet tends to break up into segments of length 2π times the jet radius. Rayleigh showed that the jet breakup is a consequence of hydrodynamic instability. Several investigators followed the pioneering work of Platau and Rayleigh. Weber (1931)[74] considered the effect of density and viscosity of the ambient fluid on jet instability. Tomotika (1935) [70] found the optimal ratio of the viscosity of the jet and the ambient fluid generating maximum disturbances. Chandrasekhar (1961) [12] showed mathematically that viscosity tends to reduce the breakup rate and increase the drop size. Taylor (1962) [66] demonstrated that the ambient viscosity has much influence on the jet breakup. He showed that for large jet velocity the drops generated by the jet breakup may be much smaller than the jet diameter, as in atomization. Several review articles have been published in this area, the latest ones by Chigier and Reitz (1996) [13] and Lin and Reitz (1998)[45].

Most of these studies are related to breakup of a liquid jet penetrating into gas environment, as for example in combustion processes. A large number of studies, related to chemical processes and mixing have been performed where liquid is penetrating

into another liquid, often immiscible. A number of studies have been performed for jet breakup under FCI conditions, where high temperature liquid jet is injected into a continuous liquid media at a lower temperature.

2.1.1 Dimensionless numbers in jet breakup

The flow of fluid jet penetrating vertically into another fluid can be characterized by a set of dimensionless numbers. The density ratio (α) is important as it determines the penetration rate of the jet head and plays an important role in the jet instability. The viscosity ratio (β) is also important, the Weber number (We), the Reynolds number (Re) and Ohnesorge number (Oh).

$$\alpha = \frac{\rho_2}{\rho_1} \tag{2.1}$$

$$\beta = \frac{\nu_2}{\nu_1} \tag{2.2}$$

$$We = \frac{\rho U^2 D}{\sigma} \tag{2.3}$$

$$Re = \frac{\rho U D}{\mu} \tag{2.4}$$

$$Oh = \frac{We^{1/2}}{Re} \tag{2.5}$$

In the case of large Reynolds and Weber numbers, the inertia force is dominating compared to viscosity and capillary forces. For a jet penetrating vertically under the influence of gravity into a fluid pool, the Froude number (Fr) may be the dominant parameter, determining the jet instability.

$$Fr = \frac{U}{(gD_j)^{1/2}} \tag{2.6}$$

2.1.2 Breakup regimes

The breakup of fluid issuing from a nozzle can be divided into five distinct breakup regimes depending on the dominant forces causing the breakup. A good way to distinguish between those regimes is to look at the coherent breakup length as a function

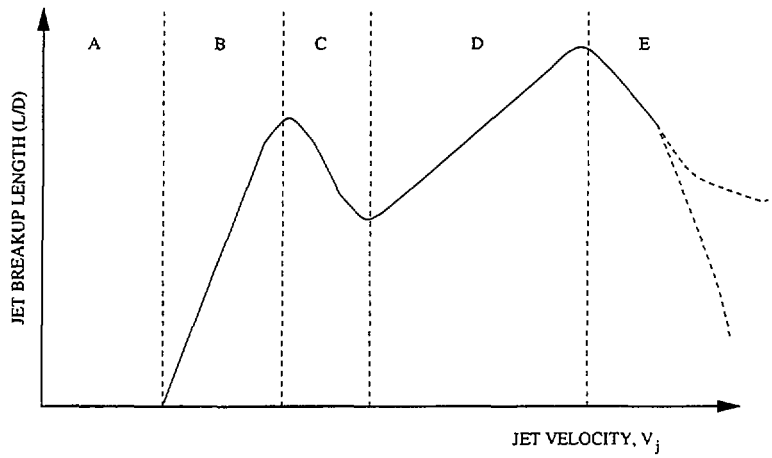

Figure 2.1: Breakup regimes: Breakup length as a function of jet velocity. A: Drop formation regime, B: Rayleigh regime, C: First wind-induced breakup or transition regime, D: Second wind-induced breakup or turbulent regime and E: atomization.

of velocity. Figure 2.1 shows the breakup length as a function of velocity for the five distinct breakup regimes A-E. The drop formation regime (A) is observed when liquid is issued steadily into an immiscible fluid at low flowrates. The formation of drops occurs at the nozzle exit similar to that of a gas bubble. As the jet velocity is increased, a critical flow is reached at which jet forms and drop starts to form at the jet end by varicose breakup, this is the Rayleigh (laminar) regime (B). This regime is dominated by growth of long wavelength, small amplitude disturbances due to the interaction between the liquid jet and the surrounding liquid. The first wind induced (transition) regime (C) is dominated by similar axisymetric long wavelengths, which induce a sinuous type of breakup. The amplitude disturbances grow as the velocity is increased. At higher velocity the second wind or turbulent induced regime is obtained (D). This regime is thought to result from the unstable growth of short wavelength waves. The breakup mechanisms are mainly due to mixing of coarse breakup mechanism and stripping from the jet body. At even higher velocity a catastrophic breakup or atomization is observed, leading to almost instant breakup upon entry into the immiscible liquid (E). Table 2.1 sumarizes the the breakup modes and droplet size for the five breakup regimes. The first three regimes (A-C) are reasonably well understood. The form of the breakup curve in these regimes can be fairly well predicted from linear stability analysis (Lin and Reitz). Beyond the first upwind (transition) regime there is more confusion about how the breakup curve looks like. Several factors, can influence the breakup phenomena, such as prior internal flow pattern caused by separation and caviatation, can become important. Those factors may explain why such discrepancy in measurements of breakup lengths has been observed. Several reviews on the jet breakup length under

Table 2.1: Breakup regimes: Breakup modes and droplet size

Regime	Breakup mode	Particle size
A) Drop formation	Capillary	Larger than orfice diameter
B) Rayleigh Laminar	Varicose	Larger than jet diameter
C) First upwind/ Transition	Sinousodial	On the order of jet diameter
D) Second upwind/ Turbulent	Surface striping/ Coarse breakup	Smaller than jet diameter
E) Atomization/ Catastrophic	Core breakup/ Wave striping	Much smaller than jet diameter

FCI conditions for both isothermal and nonisothermal conditions have been performed (see e.g. Bürger et al. [11], Gingsberg [26]). For isothermal flow, the breakup length is found to correlate with the density ratio, the Weber and the Reynolds numbers. For non-isothermal jet breakup, the density ratio and the Froude number are the most important parameters. These correlations are obtained for jet breakup in the second upwind and atomization regimes.

In this chapter, some aspects of the melt jet fragmentation during fuel coolant interactions are addressed. The first section focuses on melt jet fragmentation experiments. The experiments are divided into two parts, the first part focuses on low temperature experiment of metallic liquid jet penetrating into water. The second part focuses on breakup of oxide liquid jet at high temperature penetrating into water. In the second section the MELT-3D method is employed to investigate fragmentation of the melt jet in coolant. In particular, the computation is compared with the low temperature jet fragmentation experiments. The last section deals with numerical simulation of interfacial phenomena associated with hydrodynamic FCI.

2.2 Experimental Investigation of Jet Breakup

In this section results from experimental investigation concerning the hydrodynamic fragmentation of a melt jet in water are presented. The purpose of the study is to both identify and quantify jet fragmentation characteristics, placing particular emphasis upon the impact of melt and coolant thermal-hydraulic conditions on the size distri-

bution of the resulting debris particles. The approach is to perform experiments, with various simulant materials, at different scales, under different conditions, with variation of controlling parameters affecting the jet fragmentation processes. The jet experiments are divided into two parts, low temperature experiments and high temperature experiments.

2.2.1 Low temperature experiments

A systematic investigation of the effect of coolant and melt thermal-hydraulic conditions and of melt physical properties upon jet fragmentation and particle debris characteristics (shape & size) was performed. A set of 21 experiments were conducted employing the low melting point alloy, cerrobend-70, as jet fluid. Two melt jet diameters of 15 and 25 mm were used and the gravity-driven jet velocity was varied up to 5 m/s. Melt masses of as much as 70 kg ensured long jet discharge time frames (up to 16 s.) and thus a quasi-steady jet fragmentation process. A thorough description of the experimental facility and test procedure can be found in Appendixies A and D

Observations and Experimental Results

Jet fragmentation behavior

Figure 2.2 shows the transient behavior of the jet during penetration into the water tank. It was seen that during the initial penetration period the jet features significant fragmentation due to atomization. The Weber number, $\frac{\rho_c |U_j - U_c|^2 D_j}{\sigma}$, based on the relative jet-to-coolant velocity, is highest during this period and may reach values of 10^3 for D_j = 25 mm. However, at later times, the coolant around the jet begins to descend owing to shear forces induced by the falling jet and particle cloud. This causes stabilization of the jet in the upper region of the coolant pool, while jet atomization continues at its leading edge, as depicted in Figure 2.3.

Influence of the tube section design

The jet fragmentation behavior was observed to be similar in the cases with submerged and unsubmerged nozzles. Thus, for these experiments no noticeable effect can be attributed to air entrainment or air-space jet acceleration over the 0.4 m length.

Differences in fragmentation behaviors were observed, however, when comparing results of 25 mm diameter tubes with tube lengths of 0.3 m and 0.7 m, see Dinh et al.

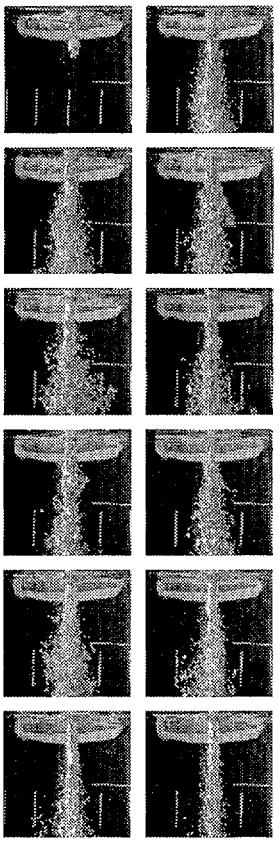

Figure 2.2: Jet fragmentation dynamics. Upper region. 25 mm jet. $U_j^o \simeq 3.5$ m/s. Time interval 80 ms between the pictures.

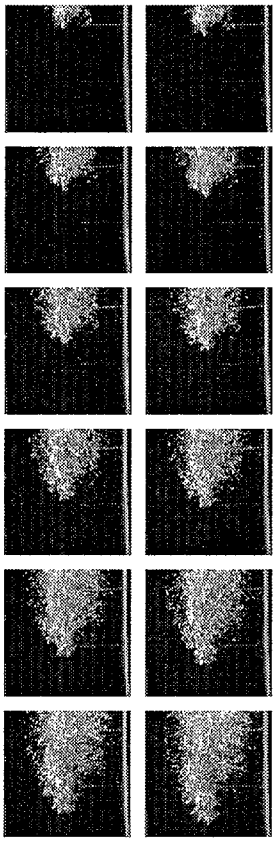

Figure 2.3: Jet fragmentation dynamics. Lower (breakup) region. 25 mm jet. $U_j^o \simeq 3.5$ m/s. Time interval 12.5 ms between the pictures.

[20]. The longer tube length appears to foster flow stabilization thus resulting in a more coherent jet in the upper regions of the water tank.

Figures 2.4 and figure 2.5 show the jet breakup with and without insertion of helical coil inside the jet tube, respectively. The coil enhanced the jet turbulence level and led to more forceful atomization patterns compared to experiments without the coil.

Particle debris analysis

The particle debris collected at the bottom of the coolant tank was classified in size using a series of varying mesh size sieves. It was found that coolant temperature significantly affects both the debris particle shape and its porosity. In particular, the

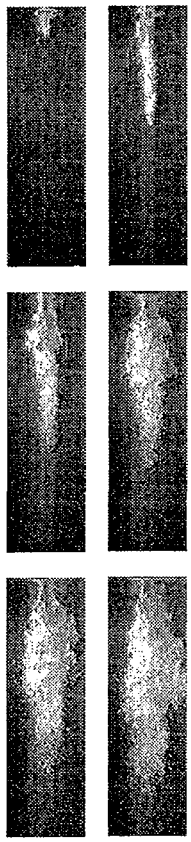

Figure 2.4: Jet fragmentation dynamics. Coil inserted into the tube. $U_j^o \simeq 3.5$ m/s. Time interval 80 ms between the pictures.

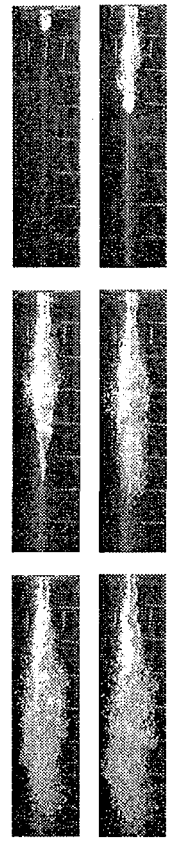

Figure 2.5: Jet fragmentation dynamics. No coil inserted into the tube. $U_j^o \simeq 3.5$ m/s. Time interval 80 ms between the pictures.

maximum size of fragments was seen to increase with decreasing coolant temperature. Distinctly different characteristics of the particle debris at different coolant temperatures can be seen in Fig.2.6 where the mass fraction represents the weight of particles with given diameter to that of the entire debris bed sample. Notably, a major fraction of the particles have large diameter for the cases of $T_c < 15°C$, while the distribution of particle masses for cases with $T_c > 40°C$ are much more uniform.

It is reasonable to expect that the characteristic time for solidification of a jet fragment would decrease with increases in the melt-to-coolant heat transfer rate. Solidification of the stripped particles would then in turn prevent any further sequential fragmentation (ignoring mechanical fragmentation mechanisms). It was found that the average

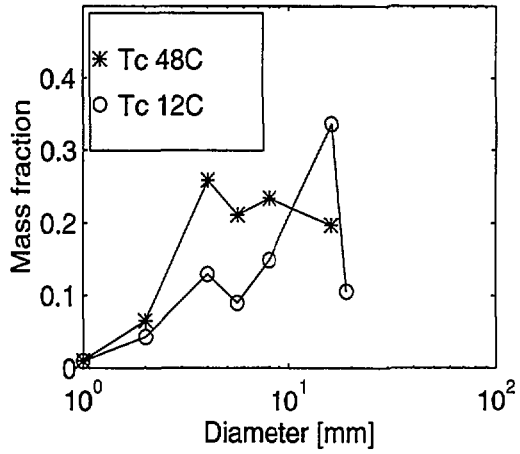

Figure 2.6: Effect of the coolant temperatures T_c (D_j = 25 mm), on particle size.

size of fragments for cases with $5 < T_c < 15^oC$ was approximately 12 to 15 mm[1]. With increasing coolant temperature ($T_c > 40^o$C) the fragments become smaller and smoother (the average size of the fragments is 3.9 to 4.5 mm). Thus, the solidification, and thereby the fragmentation is not found to be strongly dependent upon the heat transfer above the 40°C coolant temperature.

An estimate of the characteristic time for droplet fragmentation, τ_f, can be determined by the method developed by Pilch and Erdman [60].

$$\tau_f = t\frac{U_d \cdot (\rho_c/\rho_d)^{1/2}}{D_o} = f(We) \tag{2.7}$$

Where the subscript d represents droplet parameters and D_o is the initial droplet diameter. If one assumes that the originally stripped droplet has diameter of $D_o \approx 10$ mm and a velocity of ≈3 m/s then the characteristic times of breakup initiation, t_{ini}, primary breakup, t_{pri}, and total breakup, t_{tot}, as put forth in [60] become 5, 17 and 37 ms respectively.

The remaining timescale of interest is that for solidification which can be estimated by the time necessary to remove the melt superheat, $\Delta T_{sup} = T_j - T_{mp}$, and the melt heat of fusion, H_{fusion}, from a crust layer of thickness δ.

[1]The diameter of spherical drops with equivalent mass is smaller and ranges from 6 to 10 mm.

$$t_{sol} = t_{sup} + t_{fus} \tag{2.8}$$

where

$$t_{sup} = \frac{\rho_m \cdot C_{pm} \cdot \Delta T_{sup} \delta}{q"} \tag{2.9}$$

and

$$t_{fus} = \frac{\rho_m \cdot H_{fusion} \delta}{q"} \tag{2.10}$$

The heat flux is estimated as, [37].

$$q" = \frac{\kappa_c}{D_o}(2 + 0.6 \cdot Re^{0.5} \cdot Pr^{1/3})(T_j - T_c) \tag{2.11}$$

Table 2.2 shows the solidification times for the cases with water temperatures of T_c = 5°C and T_c = 45°C. The thickness of the crust layer [2] is varied between 10μm and 50μm. Such a calculation reveals that for a 20μm-crust layer in cold water, that the characteristic solidification time may be less than that of primary breakup. This supports the observed results that particle debris sizes were smaller under cold water conditions.

Table 2.2: Characteristic times of solidification to form a given crust thickness.

Crust thickness	t_{sol} (ms)	
δ (μm)	T_c = 5°C	T_c = 45°C
10	4.6	9.1
20	9.3	18.1
30	13.9	27.2
40	18.5	36.3
50	23.2	45.3

Haraldsson et al. [30] provides extended information and discussion on the effect of wired spring-like coil in the tube, as well as of other effects such as the feedback from the coolant temperature and the velocity of the jet, on the particle size distribution.

[2]The value of δ which will prohibit subsequent drop fragmentation may of course depend on melt physical properties and the flow conditions.

It should be noted that there exist inaccuracies when determining the particle size distribution with sieves [38] and this is due primarily to the non-spherical shapes of the fragments. Despite the fact that they may constitute a larger mass fraction of the debris, the surface-to-volume ratios for the larger size fragments is less. Conversely, the smaller particles exhibited smoother and more spherical shapes. The implementation of a shape factor may be necessary in future efforts in order to better characterize the interfacial area under various conditions. Nevertheless, the experimental information obtained by sieving provides good insight into the fragmentation process and fosters a method of identification of the fragmentation phenomena relevant to the experimental conditions.

Summary of Results

Coolant temperature was found to significantly affect both the shape and porosity of the debris particles. The maximum fragment size was seen to increase with reduction in coolant temperature. At coolant temperatures Tc > 40°C the fragments became smaller and smoother with an average size of 3.9 to 4.5 mm whereas in the range $5 < T_c <$ 15°C the average fragment size was 12 to 15 mm.

No effect of coolant voiding on the particle size distribution was found for gas volume fractions up to 20 % nor was any influence observed for submerged versus unsubmerged nozzles. The insertion of a helical coil into the jet tube, enhanced the jet turbulence level and showed a corresponding increase in the atomization pattern observed.

The above experiments provided a new database of hydrodynamic jet fragmentation in single and two-phase coolants for use in model (code) development and validation.

2.2.2 High temperature experiments

A series of high temperature jet fragmentation experiments were performed. The objective was to observe and quantify the jet breakup characteristics, with emphasis on delineating the roles of melt physical properties and of coolant thermal-hydraulic conditions in the breakup process. A series of 22 experiments employing three high melting point binary oxides, $CaO\text{-}B_2O_3$, $MnO\text{-}TiO_2$ and $WO_3\text{-}CaO$ were performed. The melt jet was generated from a 25 mm nozzle and the velocity, which depended on the height of melt jet free fall, was varied up to 6 m/s. Melt mass of up to 35 kg ensured a

long jet discharge time (up to 10s.), thus, quasi-steady jet breakup process. A thorough description of the experimental facility and test procedure can be found in Appendix C.

Experimental Results

Jet Dynamics

Fig. 2.7 shows the transient behaviour of the jet as it penetrates into the coolant pool. It was observed that soon after entry into water the jet undergoes significant fragmentation due to atomization. The Weber number, $\frac{\rho_c |U_j - U_c|^2 D_j}{\sigma}$, based on relative velocity between jet and coolant, is high during this period and may reach values of $5*10^3$. The temperature of the coolant pool significantly affects the initial jet dynamics

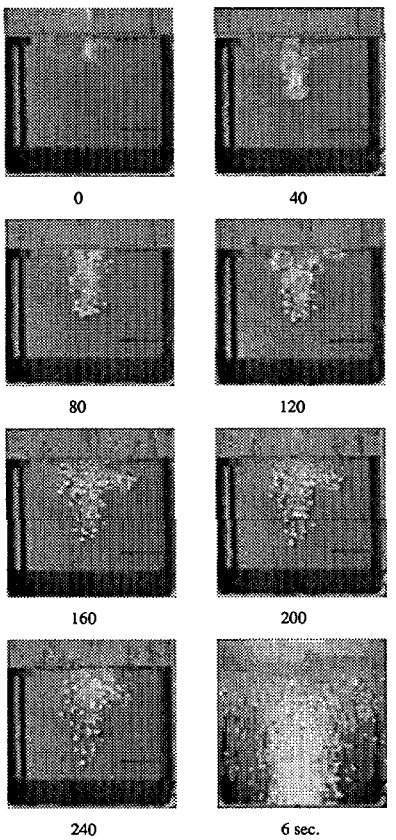

Figure 2.7: *Jet fragmentation dynamics. Jet diameter 25 mm, jet velocity U_j^o=6 m/s. Time between frames 40 ms, except last frame is 6 sec. into the process.*

and its breakup behaviour. It is observed that coolant boiling is quite violent for low

subcooling. This has significant influence on the initial jet dynamics.

Effect of Temperature

The foremost results obtained from these experiments are that the melt jet fragmentation can be classified into two regimes of either *hydrodynamics-controlled* or *solidification-controlled.* The delineation between these two regimes can be observed from the size characteristic and morphology of the solidified debris which is formed. It was found that primary determinant of which regime the jet fragmentation would fall under was the temperature of the coolant.

Figure 2.8 shows the typical morphology of fragments produced in the fragmentation-controlled regime. In this regime the jet breaks into a large number of irregular particles, coupled with very fine spherical particles. Conversely in the solidification-controlled regime, the melt jet breaks into large particles. The particles are smooth and often with hollow cavity and very brittle. Figure 2.9 shows a typical morphology of particles in the solidification controlled regime.

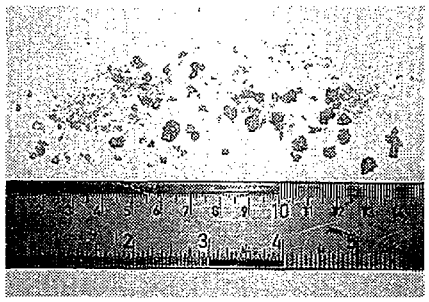

Figure 2.8: Typical morphology of the fragmentation debris in the fragmentation-controlled regime

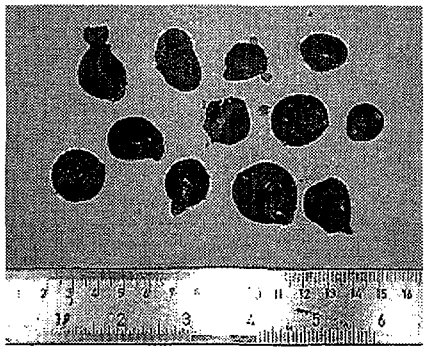

Figure 2.9: Typical morphology of the fragmentation debris in the solidification-controlled regime

Another distinct difference between those two regimes is related to the particle size distribution of the debris produced. In the hydrodynamics controlled regime, particles of different size from 0.1 mm up to the maximum size are found in the debris. However, in the solidification-controlled regime, there are mostly large particles and only few small particles. This difference can clearly be seen in Figure 2.10, which depicts the cumulative mass-size distributions of the debris produced when WO_3-CaO oxide jet interacts with water at different temperatures. In this figure, the curve with T_w=25 °C corresponds to the hydrodynamics-controlled regime, while the curve with T_w=95 °C

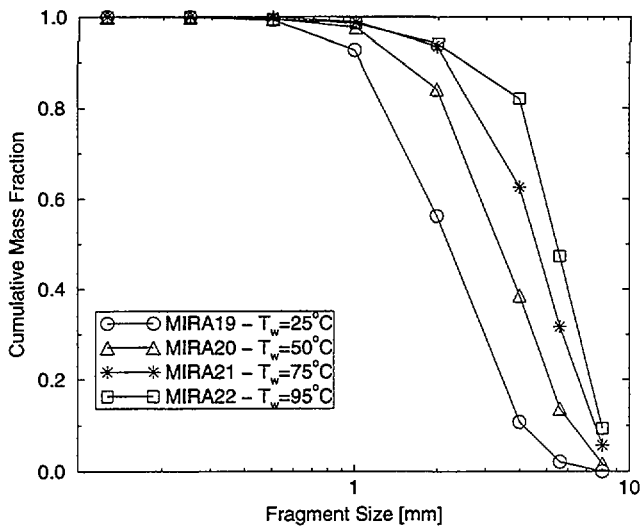

Figure 2.10: Dependence of the debris size distributions on the coolant temperature

corresponds to the solidification-controlled regime. At different coolant temperatures, the cumulative mass distributions are remarkably different.

Figure 2.11 shows the variation of the debris mass mean sizes with coolant temperature. A strong dependence of the mass mean particle size on the coolant temperature is observed for the WO_3-CaO oxide. The lower the coolant temperature, the smaller the debris mass mean size. Obviously, Figure 2.10 and Figure 2.11 together show the strong effect of the coolant temperature on the droplet fragmentation process.

Evidently, heat transfer between the melt drop and the surrounding coolant plays an important role in the melt drop-coolant interaction process under non-isothermal conditions such as were used here. In such a case, on one hand, the melt drop tends to fragment due to hydrodynamic forces. On the other hand, the drop cools down and gradually solidifies owing to heat transfer to the coolant. In its turn, solidification might suppress the hydrodynamic fragmentation, especially when the heat removal rate is very high and solidification develops rapidly. Therefore, it may be said that the coolant temperature affects the extent to which the hydrodynamic fragmentation of the melt drops could be completed under non-isothermal conditions. Accordingly, two time scales should be considered in this case. One is the fragmentation time scale, tfrag, which is the time required for a melt drop to complete hydrodynamic fragmen-

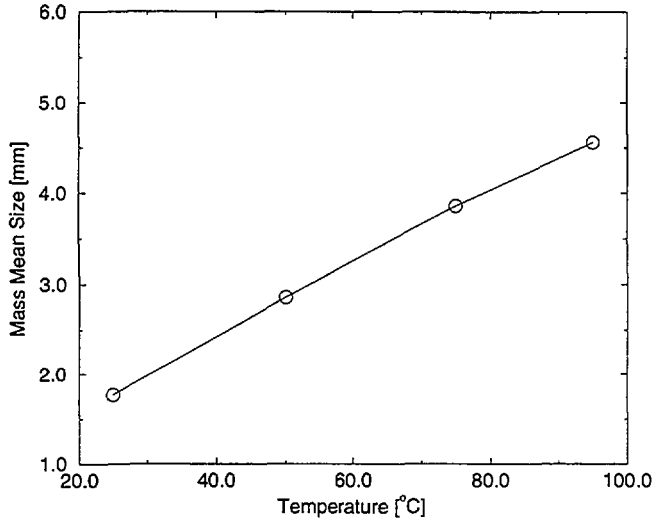

Figure 2.11: Mass mean size of the debris from the jet fragmentation tests

tation; another is the solidification time scale, t_{solid}, which is the time required for the melt drop to remove its superheat plus a fraction or all of its fusion heat, to develop partial or complete solidification. When $t_{solid} > t_{hydr}$ the hydrodynamic fragmentation process may be almost or fully complete. However, if $t_{hydr} > t_{solid}$ the hydrodynamic fragmentation process may be suppressed.

Effect of Melt Density

Cumulative mass distributions of the fragmented particles produced in the tests are compared in figure 2.12. In this figure tests performed with three different material densities are included, namely, experiments MIRA12-MIRA15, MIRA17-MIRA18 and MIRA19-MIRA22, with the corresponding densities of 2500 kg/m^3, 4300 kg/m^3 and 6500 kg/m^3, respectively. From figure 2.12 it can be seen that for all three materials, the cumulative mass distributions are sensitive to the coolant temperature. It appears that as the melt density increases smaller particles are produced during the jet breakup. Figure 2.13 shows the mass mean particle size as a function of coolant temperature. The figure shows that the density of the oxide melt has a considerable effect on the mass mean size. When the melt is of high density the mass mean size becomes smaller compared to that of lower melt density. This trend has been considered, see e.g. Nigmatullin [53] and Pilch [60], by performing analysis of a Kelvin-Helmholtz type instability on the interface of two fluids. Figure 2.14 shows the mass mean size multiplied by the square of the density ratio as a function of coolant temperature. The

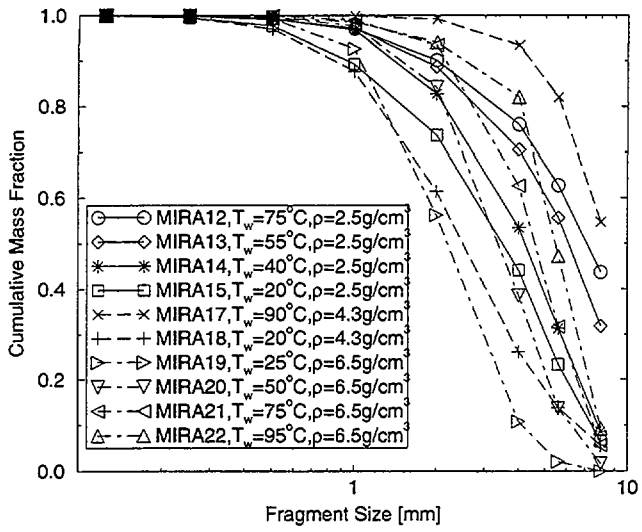

Figure 2.12: Effect of melt density on the debris size distribution

figure shows that if the square of the density difference is taken into account the mass mean diameter multiplied by the square of the density ratio is in good agreement between experiments performed with different materials. A simple correlation is obtained for the mass mean size as a function of coolant temperature and the density ratio.

$$D_{MMS} = \left(\frac{\rho_c}{\rho_m}\right)^{1/2} (0.1T_c + 2.3) \tag{2.12}$$

All the experimental data obtained in the current experiments are within +/- 25 % limit of the correlated data.

Effect of Melt Superheat

Figure 2.15 shows the cumulative mass distribution as a function of fragment size for MIRA12 and MIRA16 experiments. The melt superheat for the MIRA12 experiment is 150°C and 350°C for the MIRA16 experiments. As the superheat is increased the particles produced become larger. However, the effect of melt superheat on the particle size distribution is much less than that of coolant subcooling and than the effect of melt density.

Effect of Velocity

The velocity of the jet upon impact with the water surface was varied by changing

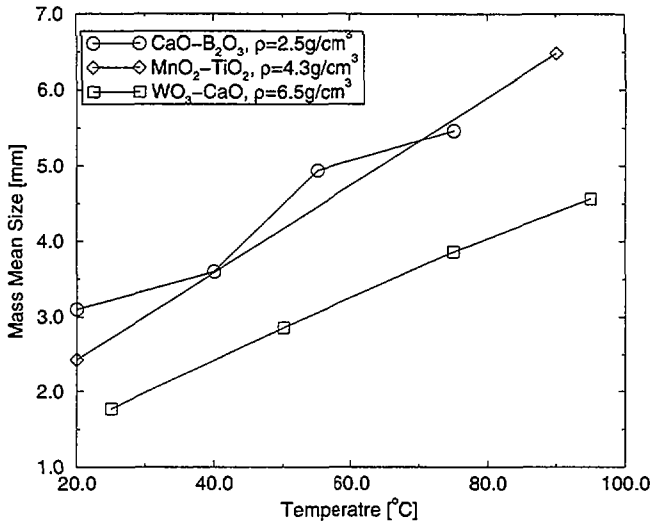

Figure 2.13: Mass mean size of the debris from jet fragmentation tests

the distance between the nozzle exit and the water surface level. The distance was varied between 0.4 m and 1.4m, obtaining velocities between 3 m/s and 6 m/s. At low velocities the jet fragmented to relatively small particles in the beginning but as the process went on the particles started to accumulate to form big clusters with no visible fragmentation. At high velocity no such accumulation was observed, the melt jet broke up completely into small size fragments. A stratification in size was observed when the debris was examined after the test. Smaller particles were at the bottom and bigger particles on top.

Summary of the Findings

The coolant temperature is found to significantly influence the characteristics of debris fragments produced from the low temperature metal jet breakup. It was found that at low subcooling the fragments are relatively large and irregular compared to smaller particles produced at high subcooling.

The melt jet density has considerable effect on the fragment size produced. As the melt density increases the fragment size becomes smaller. The mass mean size of the debris changes proportionally to the square root of the coolant to melt density ratio. This is in good agreement with theoretical stability analysis.

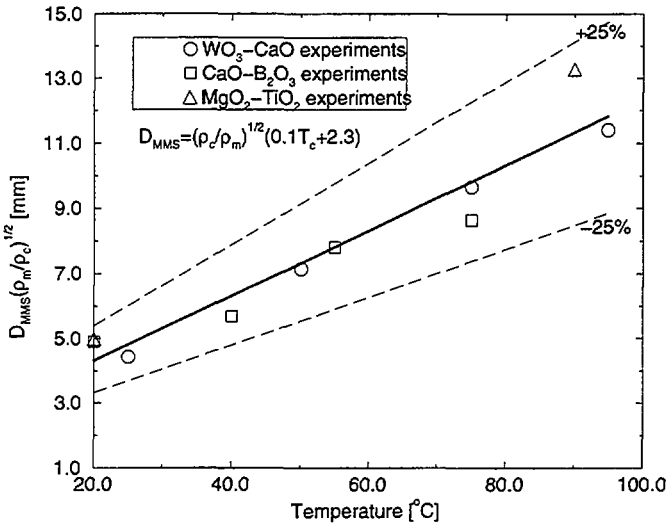

Figure 2.14: Mass mean size multiplied with the square root of melt to water density ratio as a function of coolant temperature.

The melt superheat was found to have little effect on the debris particle size distribution produced during the melt jet fragmentation.

The impingement velocity of the jet was found to have significant impact on the fragmentation process. At lower jet velocity the melt agglomerates and forms a cake of large size debris. When the jet velocity is increased more complete fragmentation is obtained.

2.2.3 Characterization of debris particles generated by FCI

The objective of present section is to compare the performance of statistical distributions which are used to describe the size distributions of fragments obtained from molten fuel coolant interactions (MFCI) experiments. Four distributions namely: (i) the lognormal [38], (ii) the upper-limit lognormal [23]; (iii) the Weibull [38]; and (iv) the Gamma-like distribution resulting from the sequential fragmentation theory (SFT) of Brown [8] are compared. A description of the size distributions and the SFT theory is given in Appendix B.

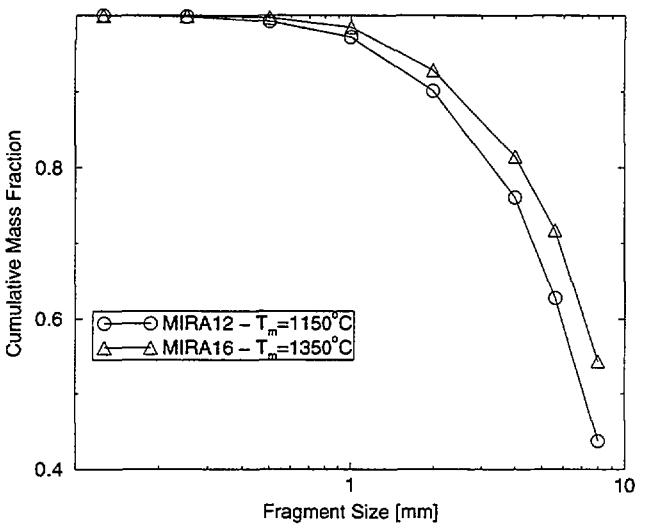

Figure 2.15: Mass mean size of the debris from jet fragmentation tests

Performance of the statistical distributions

To determine which of the four statistical distribution, mentioned above, is most suitable to fit debris data, three sets of MFCI experiments are used: One from KROTOS experiments, conducted at JRC/Ispra [48], using corium and two sets from the MIRA experiments, conducted at RIT/NPS (Appendix A and C), using cerrobend-70 and oxidic melts.

The statistical distributions are fitted to the experimental data by using non-linear regression algorithm, the Levenberg-Marquart method, which minimizes the global error function,

$$e = \sum [p_{i,exp}(l) - p_{i,fit}(l)]^2 \tag{2.13}$$

where $p_{i,exp}(l)$ and $p_{i,fit}(l)$ are the experimental and fitted number densities of the i-th observation. The unbiased estimate of the variance, $\sigma^2_{y|x}$ can be calculated from the following equation.

$$s^2 = \frac{\sum [p_{i,exp}(l) - p_{i,fit}(l)]^2}{N - \nu} \tag{2.14}$$

Here N is the total number of observed data points. The denominator, shows that ν degrees of freedom have been lost, for a ν parameter distribution. In the case of ULLN, ν is equal to three, and for SFT, LN and Weibull distributions, ν is equal to two.

A comparison between the variance of the three two-parameter distributions shows that the SFT distribution exhibits the lowest average variance, i.e. the best agreement with the size distribution data. Furthermore, a comparison between the variance of the SFT and the ULLN, for corium data, demonstrates that the average variance is lower for the SFT.

Thus, it was found that the SFT provides the best fit to the collected debris data, using a mass-average fragment size, σ (or average mass of fragments m_1), and a free parameter, γ, which indicates the deepness of the sequential fragmentation process

It should be noted that for the wide range of experimental data on debris fragments, from low temperature cerrobend-70 to high temperature corium, the SFT gives satisfactory fits to the experimental data. For experiments performed with corium at high temperature ($\sim 3000^oC$), γ was in the range from -0.76 to -0.90 and σ in the range from 1.71mm to 0.92mm. For experiments performed with cerrobend-70 at low temperature ($\sim 85^oC$), γ is in the range from -0.67 to -0.86 while σ varies 4.24mm and 14.46mm.

Parameters of the SFT

The γ parameter of the SFT is defined in terms of fractal dimension as $\gamma = -D_f/3$. The equation for the fractal dimension can be written as,

$$D_f = -3\gamma = \frac{\log(N)}{\log 1/r} \tag{2.15}$$

Where r represents fractional size and N is the number of new fragments, after each sequential fragmentation. From this equation it can be shown that, as $D_f \rightarrow 3$ the fragments are more volumemetric. As $D_f \rightarrow 2$ two dimensional shaped fragments are observed. Figures (2.16) shows the fractal dimension, as a function of mass mean diameter for the coriuma and figure (2.17) the same for cerrobend-70 and Pb-Bi data. The figures show that the fractal dimension varies between two and three depending on the shape of the debris. In the case of corium the particles become more volumetric as they become smaller. A jagged or rough debris is observed as the mass mean diameter becomes bigger. In the case of cerrobend-70 data, the SFT predicts decrease in the fractal dimension with smaller mass mean diameter.

Examination of the data, obtained from the fitting of the SFT does not give any clear correlation between the experimental conditions and the fractal dimension.

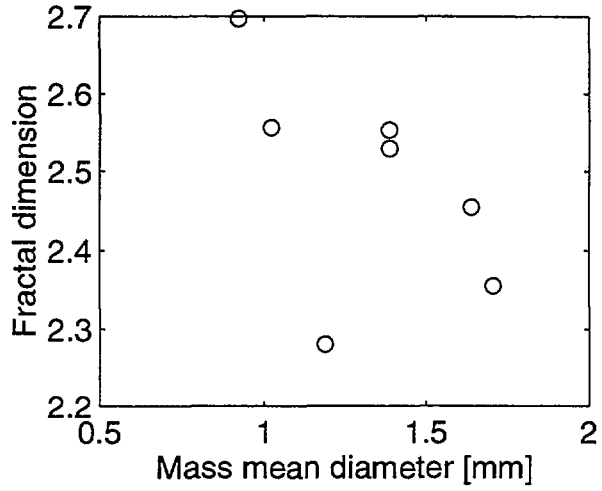

Figure 2.16: Fractal dimension as a function of mass mean diameter for corium.

2.3 Computational Simulation of Jet Breakup

2.3.1 Background

Several computational codes have been developed to simulate the premixing phase of fuel coolant interaction. In a number of codes, such as CHYMES [24] [28], IFCI [17], IVA [40] [41], MC-3D [4], PM-ALPHA [2], and others, multidimensional mixing of melt and debris phase in steam-water medium is modeled by multi-fluid Eulerian formulation. The major drawback of the Eulerian formulation is the excessive numerical diffusion of the volume fraction of the melt fluid. In order to remedy this smear-out effects of the numerical diffusion, higher order numerical schemes must be applied. However, such higher order schemes can result in oscillations and failure of the numerical scheme.

Several other codes, such as TEXAS [7], COMETA [3] and THIRMAL [15], employ Lagrangian modeling of the melt phase to simulate the premixing phase of FCI. They are restricted to one dimensional or quasi two dimensional formulations.

Recently, a new numerical approach has emerged as a powerful computational method for simulation of multiphase mixing under MFCI conditions ([20]; [54]; [19]; and [67], PM-ALPHA.L code). In this method, called MELT-3D[3], the Lagrangian

[3]**MELT-3D** stands for Multiphase Eulerian-Lagrangian Transport.

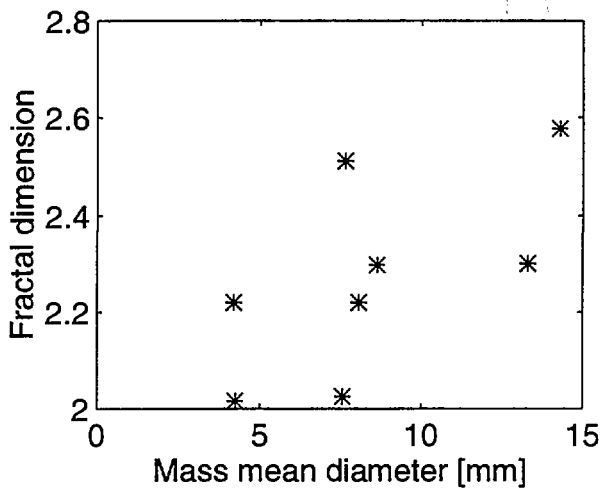

Figure 2.17: Fractal dimension as a function of mass mean diameter for cerrobend-70.

description of multidimensional transport of (melt) particles is coupled with a multidimensional Eulerian formulation of the continuum dynamics for the coolant medium. Since particle representation of the melt phase is employed, the method enables simulation of premixing stage of FCI without the difficulties associated with numerical diffusion of the melt volume fraction.

In the present study the MELT-3D approach is used to gain insight into the physics governing melt jet fragmentation and to investigate the effects of thermophysical properties on the fragmentation process. A detailed description of the computational model is given in Nourgaliev et al. [55].

2.3.2 Simulation of hydrodynamic jet fragmentation experiments

This section is devoted to the simulation of the continuous liquid jet breakup in coolant. A detailed description of the computational model is given in [55]. The results of computations are compared to the jet breakup experiments, in order to evaluate the applicability of the MELT-3D method for simulation of jet breakup process. The effects of different physical properties and of hydraulic conditions of coolant pool are examined, and the results are given in [55]. The configuration and conditions of the experiments are employed in order to compare with the experimental visualization data.

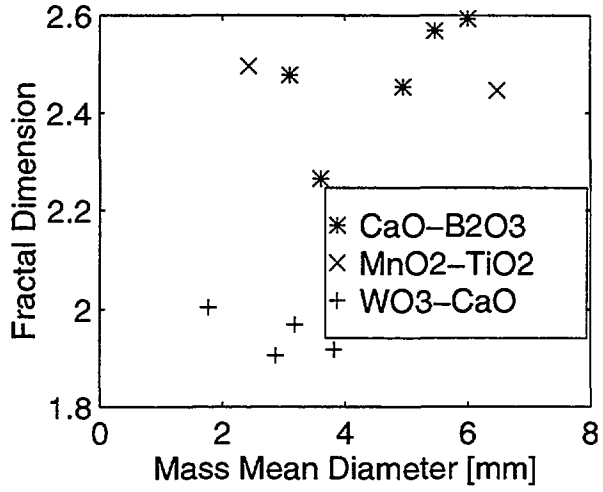

Figure 2.18: Fractal dimension as a function of mass mean diameter for oxidic melts, CaO-B_2O_3 (*), MnO-TiO_2 (X) and WO_3-CaO (+).

Dynamics of melt jet

Figure 2.19 shows the results of the simulation and experiments (exp. # 13) for the breakup of Cerrobend-70 molten metal jet in water pool. In this case, a computational grid of 35x35x40 was employed to solve the Navier Stokes equations for the Eulerian coolant field. About 700 particles of 6 mm diameter (δ_p = 6 mm), with enhanced drag coefficient (f_{C_d}) equal to 1 were used to represent the jet. Lagrangian particles are introduced in a rectangular jet, with melt volume fraction $\varphi_m = 0.8$, at the jet nozzle region. The initial jet velocity was 3.5 m/s and the jet diameter was 25 mm. The temperature of the jet and the coolant were 85^oC and 85^oC, respectively.

It can be seen that the experimental and the simulation results are in a good agreement for the dynamics of the jet. The simulation follows the leading edge advancement and the spread out of the jet seen in the experiment. Momentum exchange between the Lagrangian particles and the ambient fluid causes the particles to decelerate causing the jet to expand in area. As can be seen, in the experiment, the jet leading edge forms an arrow-like front which propagates into the coolant pool. This behaviour is also predicted by the simulation.

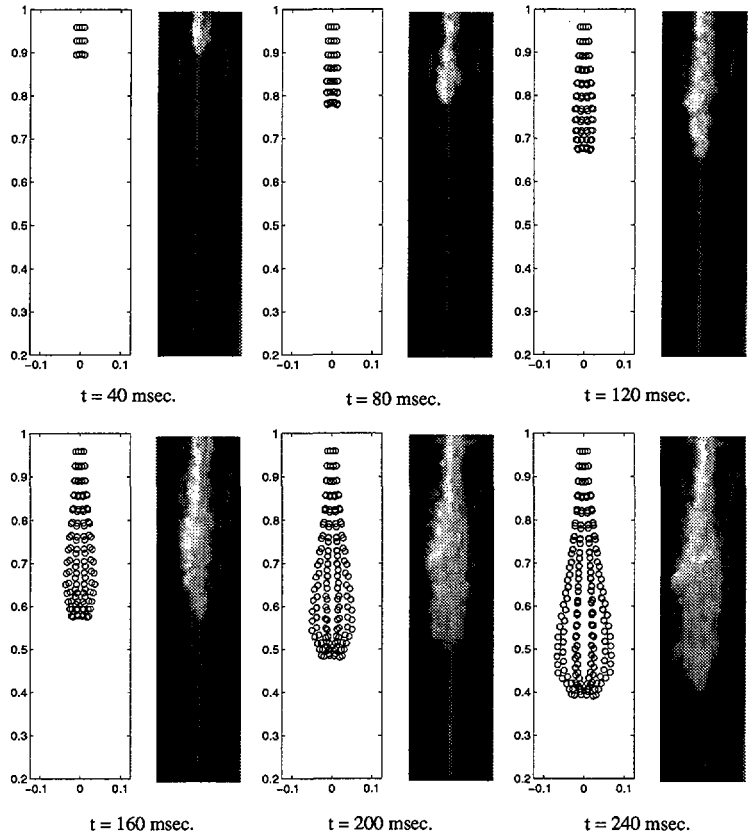

Figure 2.19: Simulation of experiment on Cerrobend jet fragmentation in water. MELT-3D calculations vs. experimental visualization (D_j = 25 mm, U_j = 3.5 m/s).

Effect of particle drag

Figure 2.20 shows comparison between experimental observations (exp. # 13 and 14) and simulation of melt jet penetration into the coolant pool as a function of time. The solid lines are MELT-3D calculations results, obtained with different values of the particle drag enhancement (f_{Cd}). In this case, the simulations were performed using 238 Lagrangian particles of 12-mm diameter. The ratio f_{C_d} was varied from 1 to 4. Results of simulations are shown along with the data obtained from two Cerrobend-70 jet experiments, [29]. The initial jet diameter, velocity and temperature were the same as above, but the coolant temperatures were varied (85^oC and 45^oC).

First, comparison of the experimental data with the computed results is shown in figure 2.20, it appears that in the experiment the drag coefficient increased as the jet

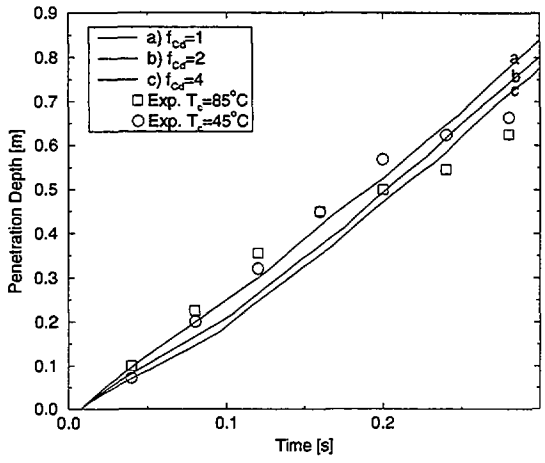

Figure 2.20: Effect of particle drag enhancement (f_{C_d}) on the jet penetration depth as a function of time for Cerrobend-70 melt jet.

penetrates deeper into the coolant pool. When the coolant pool is above 45^oC, the drag seems to follow the f_{C_d} = 1.0 line relatively well. At the end of the process, the drag begins to increase. It was noticed during the experiments, that the fragments become smaller and smoother with increased coolant temperature. At low temperature, the solidification was found to strongly affect the particle shape and size, [29]. Likely, the particles are very irregular and have complex shape which leads to higher drag enhancement factor.

Effect of particle diameter

Sensitivity study was performed to investigate the effect of the Lagrangian particle diameter on the penetration of the jet into the coolant pool. Figure 2.21 shows comparison between experimental observations (exp. # 13 and 14) and the MELT-3D simulation using 2, 4, 6, 8 and 12-mm particles. The number of particles employed in the simulation ranged from 238 particles of 12-mm diameter up to 2050 particles of 2-mm size. The drag enhancement coefficient (f_{C_d}) was set equal to 1. For comparison, we employed the same experimental data, as described above.

As can be seen from figure 2.21, calculations with particle diameter of 12 mm give the best comparison with experiment.

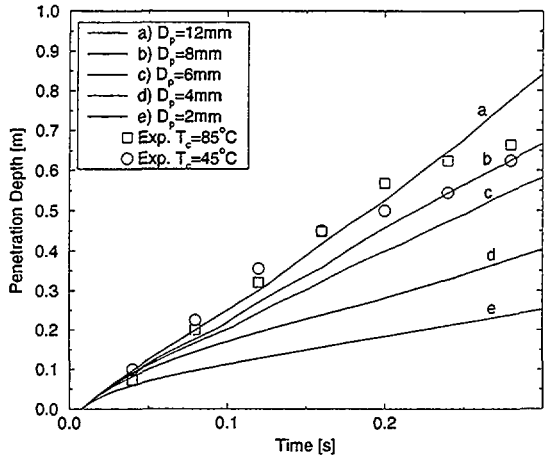

Figure 2.21: Effect of particle diameter on the jet penetration depth as a function of time for Cerrobend-70 melt jet.

The above calculated results tend to show that a varying particle size may have to be utilised to adequately model the jet fragmentation process, which involves a sequential breakup mechanism. Probably in the initial phase a large particle size (10-12 mm in the case considered) can be used, while this characteristic length (size) should decrease for a given Lagrangian particle. As a result, a multigroup treatment may be required to describe the transient increase in particle number. Also, the drag coefficient should be adapted to the local conditions. At very high jet phase volume fraction, the particle-ambient drag is nearly zero. As the initial drops fragment and solidify, the drag coefficient may significantly increase.

2.3.3 Summary of simulation results

The MELT-3D method is applied for simulation of continuous jet fragmentation. Parametric investigation of coolant properties and jet/coolant velocities demonstrated the model capabilities to analyse the complex processes of multiphase mixing. It was found that the method is computationally robust, inexpensive and does not encounter problems of excessive numerical diffusion and oscillations, which usually result from the Eulerian representation of the melt phase.

2.4 Numerical Simulation of Kelvin-Helmholtz Instabilities

2.4.1 Background and problem formulation

Kelvin-Helmholtz instabilities arise generally from a finite difference in velocities at an interface, separating two fluids, which may appear in many two-phase transportation processes. A precise understanding of non-linear evolution of Kelvin-Helmholtz instability is important in many applications. An example is the study of fuel-coolant interactions (FCIs), which may occur during the course of a severe accident in a light water reactor. The Kelvin-Helmholtz instability has significant effects on momentum, mass and heat transfer between molten fuel and coolant, and may be the dominant the melt jet and drop breakup mechanism under certain conditions.

For a long time, analytical methods (e.g. linear, non-linear, asymptotic analyses) have been developed and applied to study the physics which governs the interfacial interactions. Analytical methods are, however, not general because of the assumptions and simplifications in each particular case. This limits the applicability of the analytical models to many practical situations, involving complex (non-linear) interface structure.

Recently, several advanced numerical methods have made significant progresses in simulating fluid flows with interfaces, e.g., front-tracking method [73], volume-of-fluid (VOF) method [32] and level-set method [1] [56]. These numerical methods have been successfully employed to simulate weak and moderate interfacial interactions, e.g. bubble rise, drop deformation, jet breakup at low Weber number, etc.. Numerical solutions of intense interfacial interactions, however, suffer from both physical and numerical instabilities and are strongly grid-dependent. For example, it was observed in [9], [63] that the interface develops numerous small-scale instabilities, as the spatial resolution increases.

In this section, the level-set method is used to investigate the effect of surface tension and viscosity on the development of Kelvin-Helmholtz instability. A detailed description of the computational model is given in appendix E.

2.4.2 Effect of Physical Properties

Effect of surface tension

In this section, we study the effect of surface tension on the evolution of Kelvin-Helmholtz instability from a near equilibrium condition ($\epsilon = A_0/\lambda_{ini} = 0.01 \ll 1$). The two fluid considered in the present calculations are inviscid, and density matched ($\rho_1 = \rho_2 = \rho$). The initial velocities in the upper and lower fluid layers are $U_1 = U$, and $U_2 = -U$, respectively.

Based on inviscid linear stability analysis [12], it was found that with initial perturbation $e^{i(kx-\omega t)}$, the dispersion relation is:

$$D(\omega, k) = -k^2\sigma + k^{-1}\rho(i\omega - kU)^2 + k^{-1}\rho(i\omega + kU)^2 = 0 \tag{2.16}$$

Thus, the growth rate for perturbations is given by:

$$\omega^2 = (\frac{2\pi}{\lambda})^2 U^2 (1 - \frac{4\pi k}{We}) \tag{2.17}$$

It can be seen from equation 2.17 that the surface tension will suppress the instability when the wavenumber k is larger than $We/4\pi$. For wavenumbers $0 < k < We/4\pi$ the perturbations will grow unlimited. By differentiating equation 2.17, the maximum growth rate is obtained at $k = We/6\pi$.

The critical Weber number We_c is $4\pi \simeq 12.6$. If $We < We_c$, no perturbation will grow. Figure 2.22 compares the evolution of the interface with $We = 10 < We_c$, $We = 50 > We_c$ and $We = 80 > We_c$ at the dimensionless time, $t^* = t(U_1 - U_2)/\lambda_{ini} = 2$. Both simulations employ a 256×256 grid and $\Delta t^* = 1.25 \times 10^{-4} s$. For $We = 10$, the initial perturbation does not grow; the surface tension initially damps the wave motion and then the inertia induces the wave again. For $We = 50$, the perturbation amplitude increases significantly in time. The interface deforms into finger-like shape that penetrates each fluid into the other. For $We = 80$ the interface rolls-up and Kelvin-Helmholtz instability appears on the interface. Hou et al. [34] performed vortex sheet simulations of inviscid Kelvin-Helmholtz instability and obtained a transition to roll-up regime at $We \simeq 60$.

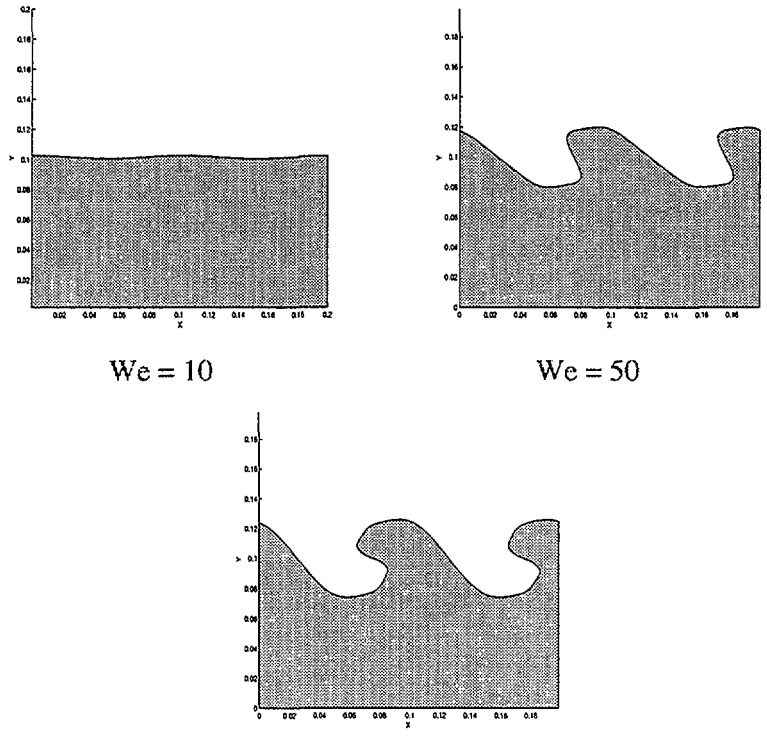

Figure 2.22: *The interface structure at* $t^* = 2$, *for,* $We = 10$, $We = 50$ *and* $We = 80$.

Effect of viscosity

The presence of viscosity may have significant effect on the evolution of Kelvin-Helmholtz instability. Viscous force, similar to surface tension force, acts against the destabilising effect of inertia. Unlike the surface tension force, which is local and acts only at the interface, the viscous force acts globally and continuously extracts perturbation energy from the fluids. The effect of viscosity on the evolution of the interface is usually represented by the Ohnesorge number. The Ohnesorge number Oh measures the viscous dissipation versus the dispersive stabilization associated with the surface tension.

In this section, we study the effect of Ohnesorge number on the evolution of Kelvin-Helmholtz instability. All simulations are performed on a 128×128 grid, which is fine enough to capture the long-time evolution of the interface. Other boundary and initial conditions are similar to those employed in the previous section.

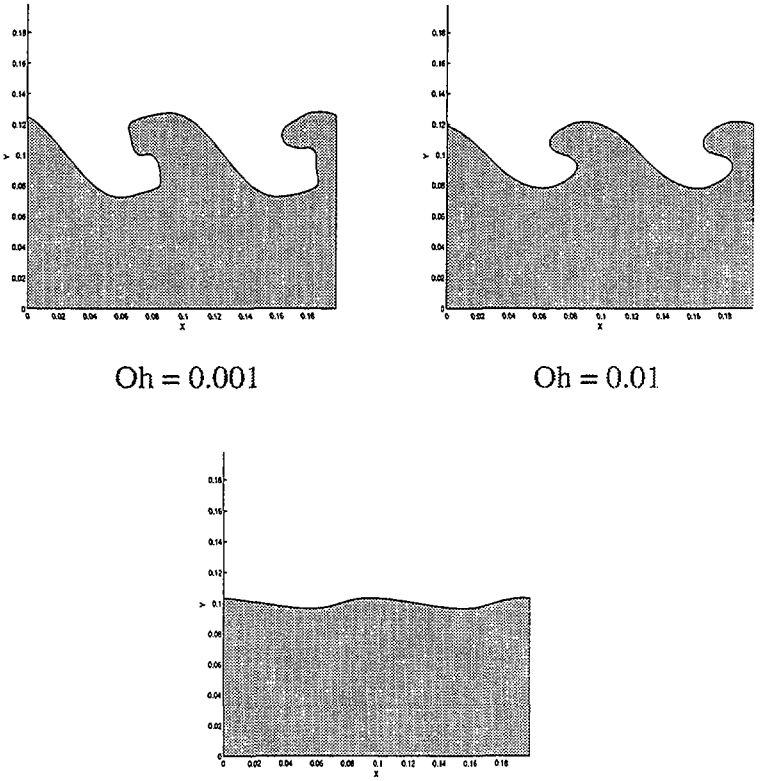

Oh = 0.001 Oh = 0.01

Oh = 0.1

Figure 2.23: *The interface structure at* $t^* = 2$, *for* $We = 200$, *and* $Oh = 10^{-3}, 10^{-2}$ *and* 10^{-1}.

In figure 2.23, the effect of viscosity on the evolution of Kelvin-Helmholtz instability at high Weber number is demonstrated, The interface structure is shown at $t^* = 2$ for $We = 200$, at three distinct values $Oh = 10^{-3}, 10^{-2}$ and 10^{-1}. A well-defined Kelvin-Helmholtz roll-up structure is observed at $Oh = 10^{-3}$, and $Oh = 10^{-2}$. Apparently, the viscosity does not have a significant effect on the shape and hydrodynamic state of the interface. Instead, the main effect of viscosity on the evolution of Kelvin-Helmholtz instability seems to be reduction of the deformation rate of the interface. This behaviour allows more time for interface relaxation to the vortices, tending to reduce the acceleration, and thus the driving potential for Kelvin-Helmholtz instability. The presence of viscosity also appears to damp the small-scale instabilities, observed in numerical simulations of inviscid Kelvin-Helmholtz instability.

2.4.3 Evolutionary regime

In the previous sections, we have seen that the evolution of Kelvin-Helmholtz instability depends on We and Oh numbers. The transient behaviour of the interface can be classified into the following *evolutionary regimes*:

- **Oscillatory regime**: the effects of viscous dissipation and dispersive stabilization associated with the surface tension inhibit the initial perturbation to grow, and cause the interface to oscillate. In the presence of viscosity, the interface finally becomes undisturbed after several oscillation periods.
- **Fingering regime** : inertia induces the initial perturbation to grow. The wave amplitude increases in time. At the later stage of the evolution, the interface deforms into elongated fingers.
- **Roll-up regime** : when the wave grows to a certain amplitude, a complex structure, known as Kelvin-Helmholtz roll-up, appears. At the later stage of the evolution, topological singularities, such as pinching-off of fluid mass or collision of fluid interfaces, may appear.

Based on results of more than 30 simulations of Kelvin-Helmholtz instability, an evolution regime map, showing transitions of evolutionary regime as function of We and Oh, is presented in figure 2.24. The most interesting feature of figure 2.24 is that while the We number required for particular finger and roll-up regime transitions remain relatively constant for small Oh ($Oh < 10^{-2}$), the We required for the various transitions progressively increase (almost square) with increasing Oh at larger Oh ($Oh > 10^{-2}$). The onset of finger and roll-up occur at We of roughly 13 and 60, respectively for $Oh < 10^{-2}$. However, roll-up is no longer observed for $We < 2500$ when $Oh \geq 10^{-1}$ while growth disappears for $We \leq 400$ when $Oh \geq 0.2$. Clearly, it is crucial to establish whether large Oh implies no growth or roll-up, or simply large values of We required for the transitions. A simple linear analysis is performed next to gain more insight into the effects of Oh on evolution of Kelvin-Helmholtz instability.

To account for the effect of viscous dissipation, we add $-4i\rho\nu\omega k$ to the right-hand side of equation (2.16). The new dispersion $D(\omega, k) = 0$ is

$$-k^2\sigma + k^{-1}\rho(i\omega - kU)^2 + k^{-1}\rho(i\omega + kU)^2 - 4i\rho\nu\omega k = 0 \qquad (2.18)$$

Solving equation (2.18) with respect to ω yields

$$\omega = -2i\nu k^2 \pm 2k(U^2 - \nu^2 k^2 - \frac{k\sigma}{2\rho})^{1/2} \tag{2.19}$$

The condition for instability, thus, is:

$$U^2 > \nu^2 k^2 + \frac{k\sigma}{2\rho} \tag{2.20}$$

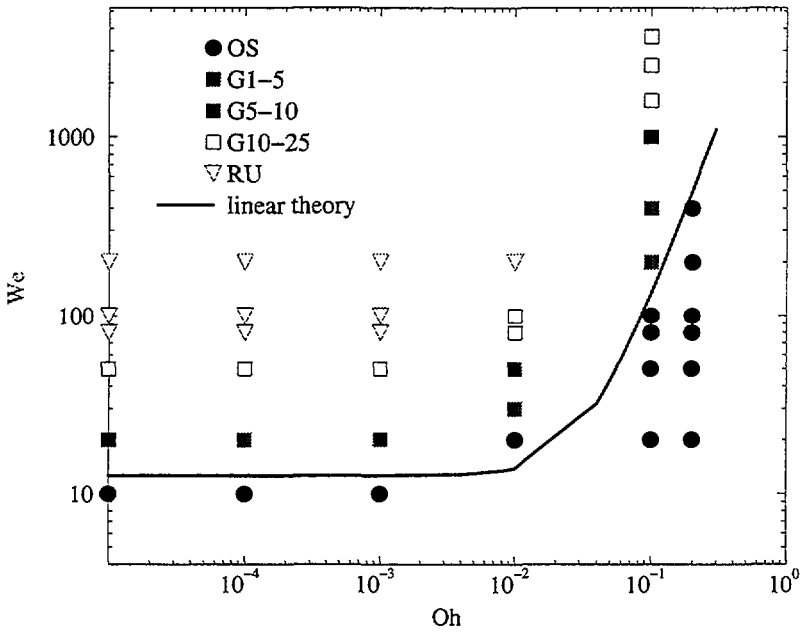

Figure 2.24: *Evolutionary regime map for Kelvin-Helmholtz instability (OS: oscillatory regime; G 1-5: transition from oscillatory to fingering regime, the wave amplitude at $t^* = 2$ is 1 to 5 times larger than the initial amplitude; G 5-10, and G 10-25, are in the fingering regime: similar to G 1-5; RU: roll-up regime).*

Substitution of $We = 4\rho U^2/\sigma$, $Oh = (\nu\rho^{1/2})/(\sigma^{1/2}\lambda_{ini}^{1/2})$, and $k = 2\pi/\lambda_{ini}$ yields

$$We > 4\pi + (4\pi)^2 Oh^2 \tag{2.21}$$

Thus, the required We_{cr} for the onset of growth can be evaluated from the conservative estimation of the linear instability analysis

$$We_{cr}(Oh) = 4\pi + K^2 Oh^2 \tag{2.22}$$

$K = 100 \div 120$ yields best-fit predicted transitions from oscillatory regime to fingering regime. This value is one order-of-magnitude higher than that predicted by linear analysis. Notably, equation (2.22) suggests that $We_{cr} \sim Oh^2$ at large Oh ($Oh > 0.1$) rather than an ultimate limit for growth at large Oh. A similar trend is observed in drop breakup experiments, in which, progressively larger We are required for the onset of drop deformation and breakup at large Oh [35] [59].

2.5 Chapter Summary

The work presented in this chapter of the thesis is focused on improving the understanding of the physics of the initial premixing phase of molten fuel coolant interactions. The experiments performed in the first part are mainly concerned with the effect of physical and hydrodynamical properties on the fragmentation process. Specifically, the effects of coolant subcooling, melt jet superheat and melt jet velocity were investigated. The debris, obtained from the jet fragmentation process, was sieved and compared to four different statistical size distributions.

In the second part, the MELT-3D algorithm was used to simulate the low temperature melt jet fragmentation experiments, reported in part one. The effect of particle diameter and particle drag on the penetration dynamics was investigated.

The direct numerical simulation presented in the third part is mainly concerned with hydrodynamic interfacial interactions. The modeling method is based on the direct simulation of the flow and interface motion, which is coupled with the level-set algorithm to eliminate numerical diffusion. The simulations of the Kelvin-Helmholtz instabilities are compared to linear stability analysis and evolutionary regimes are identified.

Chapter 3

Breakup of Liquid Drops in Liquid Media with Heat Transfer

3.1 Background and Problem Formulation

The behaviour of melt drops in coolant is a key phenomenon which governs the dynamics and energetics of melt-coolant interactions. Deformation and fragmentation of a melt droplet in a flow field has been investigated, both experimentally and theoretically, by a number of authors. A large number of experiments involving drop breakup in gas/air streams have been reported. An extensive review of experimental data and theoretical concepts related to breakup of liquid drops in liquid-gas and liquid-liquid systems was performed by Pilch (1981) [59], Pilch and Erdman (1987) [60] and Gelfand [25]. Different breakup mechanisms and modes were identified, depending on the initial Weber number. Namely, (i) vibrational breakup ($We \leq 12$); (ii) bag breakup ($12 < We \leq 50$); (iii) bag-and-stamen breakup ($50 < We \leq 100$); (iv) sheet stripping ($100 < We \leq 350$); (v) wave crest stripping ($We > 350$); followed by (vi) catastrophic breakup [60]. This regime map was based on observations obtained from experiments of liquid-drop breakup in gas (air) stream. There were very few experiments performed in liquid-liquid systems, and the related data is difficult to interpret because the breakup mechanisms have not been reported [59]. Kim [39] reported that for breakup of liquid gallium drops in water the early pulverisation modes were not observed as for liquid/gas system. Yuen et al. (1994) [80] proposed to correlate fragmentation data in liquid-liquid systems in terms of melt-coolant mixing volume. A fragmentation coefficient, β_f, was derived from high speed pictures obtained from gallium/water experiments

(Chen et al., 1995 [14]) and mercury/water experiments (Patel and Theofanous, 1981 [58]). Hsiang and Faeth (1995) [35] provided data on drop deformation and breakup in some liquid-liquid systems (water/oil; glycol/oil and glycerol/oil, with density ratios ρ_d/ρ_a equal to 1.15, 1.27 and 1.40, respectively). A dome- and bowl-shaped drop regime map was established, depending on Weber ($We = \rho_a \cdot U^2 \cdot D/\sigma$) and Reynolds ($Re = U \cdot D/\nu_a$) numbers. Recently, Gelfand [25] proposed four different breakup mode for liquid-liquid system based on experimental data reviewed in the literature. He reasons that the intermediate breakup modes reduce or disappear because of the dense liquid surrounding as observed in gas flow.

It is a common consensus that two interaction processes between melt drops and the ambient coolant, i.e., a hydrodynamic interactions due to velocity lag and a thermodynamic interactions due to non-isothermal conditions, may go on parallel under MFCI conditions. Effect of melt drop freezing was investigated, theoretically and experimentally, by Okkonen and Sehgal [57], and it was found that high surface tension in the mushy zone (temperature interval between the solidus and liquidus of the melt) may limit the deformation and fragmentation of melt drops. In addition, gas entrainment and film boiling were found to have mitigating effects on the acceleration-induced deformation process. Experiments, conducted at the JRC, Ispra in Italy, employing high temperature alumina melt and binary oxidic melt of urania-zirconia, showed significantly different explosion potential [36]. Among other mechanisms, different solidification behaviour of these melt mixtures is hypothesized to be responsible for the difference in the degree of their individual fragmentation in triggered or propagated-explosion events.

3.2 Experimental Investigations of Drop Breakup

Drop fragmentation experiments were performed using Pb-Bi alloys at both eutectic and non-eutectic compositions. Emphasis was directed towards delineating the roles which melt-to-coolant heat transfer, melt solidification, melt fusion heat and melt mushy zone play in the fragmentation process. The strong impact of coolant temperature upon fragmentation is addressed, along with the effects of droplet superheat and hydrodynamics (i.e. Weber number). Over 50 experiments (9 series) were conducted employing Lead (Pb)-Bismuth (Bi) alloys, as the melt simulant and water as coolant fluid. Figure 3.1 shows the phase diagram for Pb-Bi and the conditions for each of the experimental series. A thorough description of the test facility, experimental setup and experimental conditions can be found in Appendix F.

Debris obtained in each test was collected, dried and then classified by using a nest

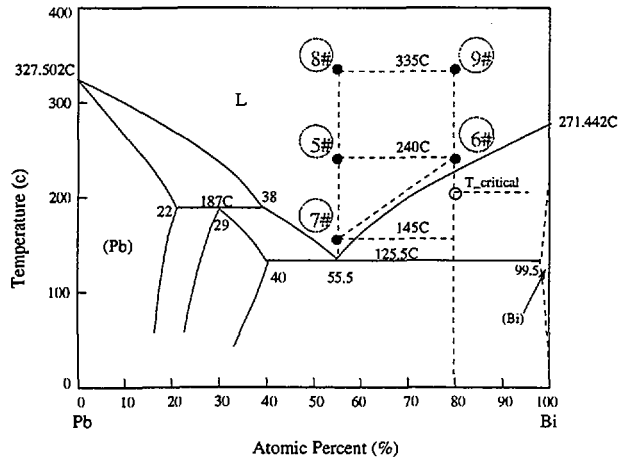

Figure 3.1: Phase diagram of Pb-Bi alloy

of sieves. Based on the cumulative mass distributions, and the mass-median size, of the solidified droplet debris obtained, characteristics of the droplet fragmentation were analysed and clarified. Analysis was performed to examine the potential effect of the changing melt properties, such as the melt enthalpy and the melt viscosity on the drop fragmentation characteristics, during the droplet cooling and solidification processes.

3.2.1 Effect of the Coolant Temperature

The foremost result obtained from these experiments is that the melt fragmentation of the alloy in water can be classified into regimes of either ***freezing-controlled*** or ***fragmentation-controlled***. The delimitation between these two regimes is easily realised from the morphology and size characterization of the solidified debris which is formed. It was found that a primary determinant of which regime the droplet fragmentation would fall under, was the temperature of the coolant.

In the freezing-controlled regime, the melt droplet deforms into sharp, paper-like particles, or irregular, long filaments, and then freezes quickly in the coolant pool. A very small portion of the drop is peeled off from the parent droplet into a number of fine particles (less than 1mm), which are smoothed, and roughly spherical. The typical morphology of the fragments collected in this regime is shown in Figure 3.2. Conversely, in the fragmentation-controlled regime, the melt droplet breaks up into a large number of irregular particles, coupled with very fine, spherical particles; and the total number of particles produced during the fragmentation process is considerably greater than those produced in the freezing-controlled regime. The typical morphology

of the debris produced in the fragmentation-controlled regime is depicted in Figure 3.3.

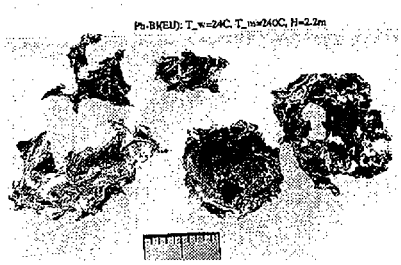

Figure 3.2: Typical morphology of the fragmented debris in the freezing-controlled regime

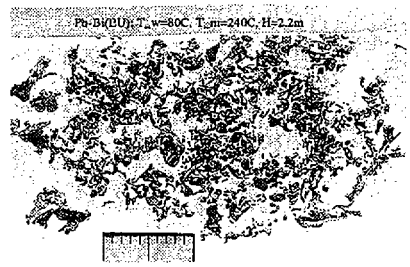

Figure 3.3: Typical morphology of the fragmented debris in the fragmentation-controlled regime

Another distinct difference between these two regimes is related to the debris size distribution. In the fragmentation-controlled regime, particles of different sizes, from 0.1 mm up to the maximum size, are found in the debris. However, in the freezing-controlled regime, there are, mostly large, irregular, particles and only a few very small particles. This difference can clearly be seen in Figure 3.4, which depicts the cumulative mass-size distributions of the debris produced when eutectic Pb-Bi drops interact with coolant at different temperatures. In this figure, the curve with T_w=24 ^oC corresponds to the freezing-controlled regime, while the curve with T_w=80 ^oC corresponds to the fragmentation-controlled regime. At different coolant temperatures, the cumulative mass distributions are remarkably different.

Figure 3.5 shows the variation of the debris mass mean sizes with coolant temperature. A strong dependence of the mass mean particle size on the coolant temperature is observed for the eutectic mixture. The lower the coolant temperature, the larger the debris mass mean size. Obviously, Figure 3.4 and Figure 3.5 together show the strong effect of the coolant temperature on the droplet fragmentation process. This observation is applied to the result of experiments with both the eutectic melt drops and the superheated non-eutectic melt drops, even at different free fall height (which affects the Weber number).

Evidently, heat transfer between the melt drop and the surrounding coolant plays an important role in the melt drop-coolant interaction process under non-isothermal conditions. In such a case, on one hand, the melt drop tends to fragment due to hydrodynamic impact. On the other hand, the drop cools down and gradually solidifies owing to heat transfer to the coolant. In its turn, solidification might suppress the hydrodynamic fragmentation, especially when the heat removal rate is very high and solidification develops rapidly. Therefore, it may be said that the coolant temperature affects the extent to which the hydrodynamic fragmentation of the melt drops could be

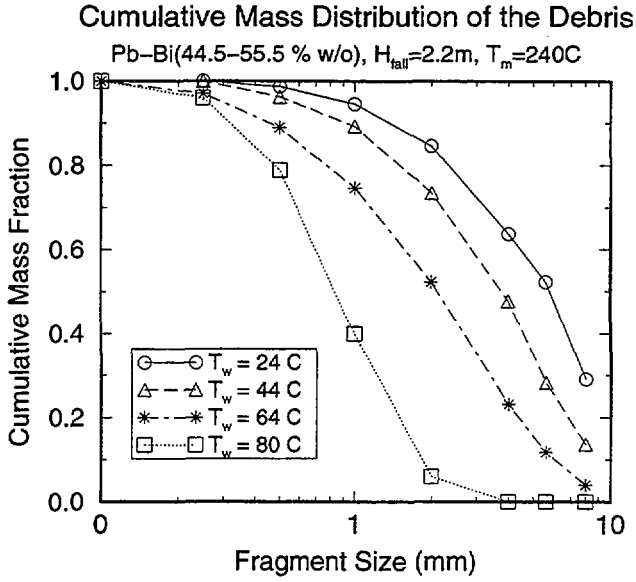

Figure 3.4: Dependence of the debris size distributions on the coolant temperature

completed under non-isothermal conditions. Accordingly, two time scales should be considered in this case. One is the fragmentation time scale, t_{frag}, which is the time required for a melt drop to complete hydrodynamic fragmentation; another is the solidification time scale, t_{solid}, which is the time required for the melt drop to remove its superheat plus a fraction or all of its fusion heat, to develop partial or complete solidification. When $t_{frag} \leq t_{solid}$, the hydrodynamic fragmentation process may be almost or fully complete. However, if $t_{frag} > t_{solid}$, the hydrodynamic fragmentation process may be suppressed.

3.2.2 Effect of the Melt Superheat

Cumulative mass distributions of the fragmented particles produced in tests with eutectic Pb-Bi alloy are compared in Figure 3.6. In this figure, three test series are included, namely, series #7,#5, and #8, with the corresponding melt superheat being 20K, 115K and 210K, respectively, as shown in Figure 3.1. From Figure 3.6, it can be seen that, in all the three cases, the cumulative mass distributions are sensitive to the coolant temperature, and that the dependencies of the mass distributions on the coolant temperature are similar. However, it appears that the higher the melt superheat, the more sensitive the fragment size distributions are to the coolant temperature.

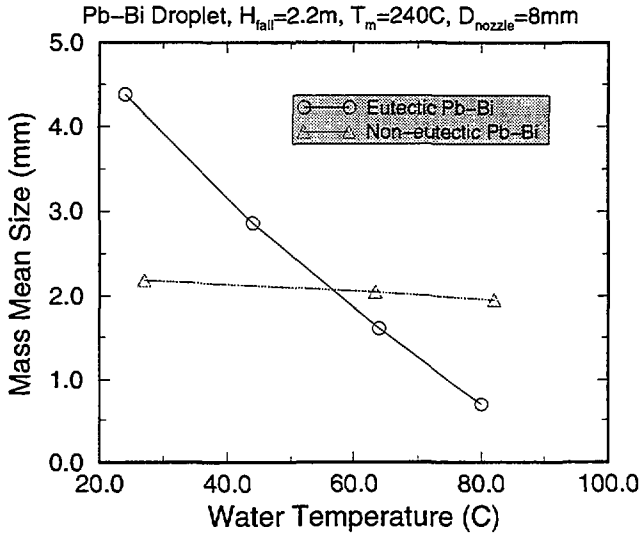

Figure 3.5: Mass mean size of the debris from droplet fragmentation tests

Cumulative mass distributions of the non-eutectic debris produced at different initial melt superheats are shown in Figure 3.7, which, again, evidence the similar effect of the melt superheat on the cumulative mass distributions as found for the eutectic melt (Figure 3.6).

Generally speaking, melt superheat determines the solidification time scale t_{solid}, which may compete with the drop fragmentation time scale t_{frag} and, therefore, affect the completeness/deepness of the fragmentation process. However, it should be noted that the solidification time scale is also influenced by the melt-coolant heat transfer rate, which depends on the heat transfer regime occurring on the drop surface. It is known that both the coolant subcooling and melt surface conditions would affect the MFBT (Minimum Film Boiling Temperature) [76], and, therefore, alter the boiling and the heat transfer modes. Additionally, different boiling conditions may result in different steam production rate, which influence the drop deceleration and fragmentation processes.

3.2.3 Effect of the Fusion Heat of the Pb-Bi Alloys

The variation of melt enthalpy with temperature for both the eutectic and the non-eutectic Pb-Bi alloys has been calculated and is shown in Figure 3.8. Using this data the fusion heat of both melts, and the amount of heat evolved when the melts are cooled

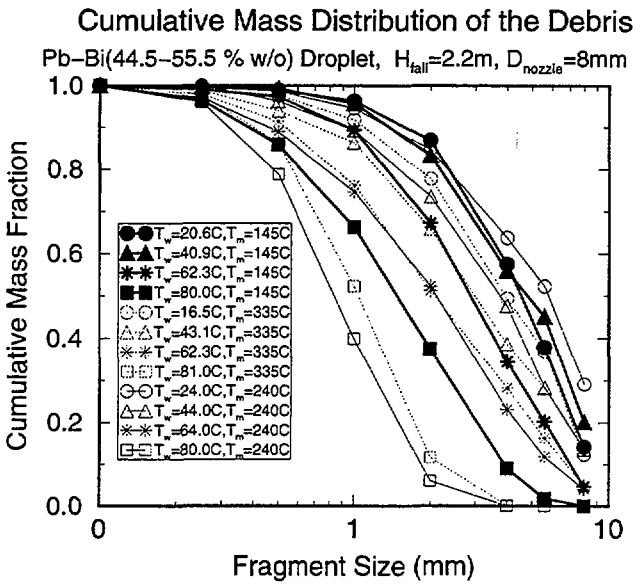

Figure 3.6: Effect of the melt superheats of the eutectic Pb-Bi alloy

down from an initial temperature T_1 to a lower temperature T_2, i.e. Q_{T1-T2}, are determined and listed in Table 3.1. It is seen that the fusion heat and the amount of heat evolved in the cooling and solidification process of the non-eutectic melt are much higher than in the eutectic alloy. Assuming other test conditions are identical, it is anticipated that a non-eutectic drop would take longer to solidify, and consequently, experience deeper hydrodynamic fragmentation than for a eutectic drop.

Figure 3.9 shows the cumulative mass distributions of the non-eutectic debris produced in test series #6, in comparison to that of the eutectic debris collected in test series #5. Surprisingly, the mass distributions of the non-eutectic debris are much less sensitive to the coolant temperature than that of the eutectic one. This is also seen in Figure 3.5, where the mass mean sizes of the non-eutectic debris are nearly the same at different coolant temperatures, but fall somewhere near the middle of the maximum and minimum of the mass mean sizes of the eutectic debris. This result implies that the hydrodynamic fragmentation of the non-eutectic melt drops is likely suppressed at an early stage by another mechanism. Most likely, the physical properties of the melt in the region between solidus and liquidus of the non-eutectic melt (termed as "mushy zone") may have relevance to this mechanism.

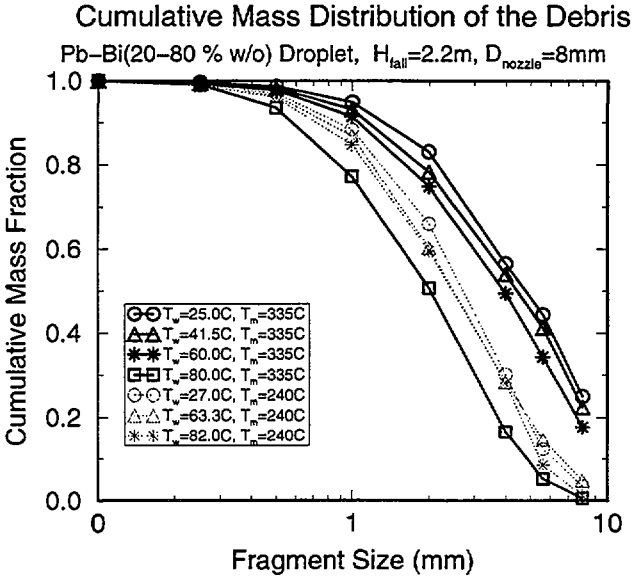

Figure 3.7: Effect of the melt superheats of the non-eutectic Pb-Bi alloy (series #6 versus series #9)

Table 3.1: Heat Evolved in the Cooling Process (J/kg)

Properties	Eutectic Pb-Bi (44.5-55.5 wt-%)	Non-eutectic Pb-Bi (20-80 wt-%)
Fusion	23540.3	50911.5
$Q_{240-125(s)}$	38864.9	53696.0

3.2.4 Effect of the Binary Alloy Mushy Zone

The obvious difference between the eutectic and the non-eutectic melts used here is that there exists a large temperature interval between the liquidus and the solidus of the non-eutectic melt (the "mushy zone"). According to knowledge about chemical-thermodynamics of materials, melt in this zone is actually a mixture of liquid melt and fine solid particles precipitated in the preceding cooling process [46]. Therefore, the viscosity of the non-eutectic melt in this "mushy zone" is dramatically higher than that of the non-eutectic melt above the liquidus temperature. That is to say, in the course of cooling, once the temperature of the non-eutectic drop falls into the "mushy zone", the drop will become increasingly viscous. At a critical temperature point (assuming it $T_{critical}$, as shown in Figure 3.1), the high viscosity of the melt will prevent the drop from further deforming and fragmenting.

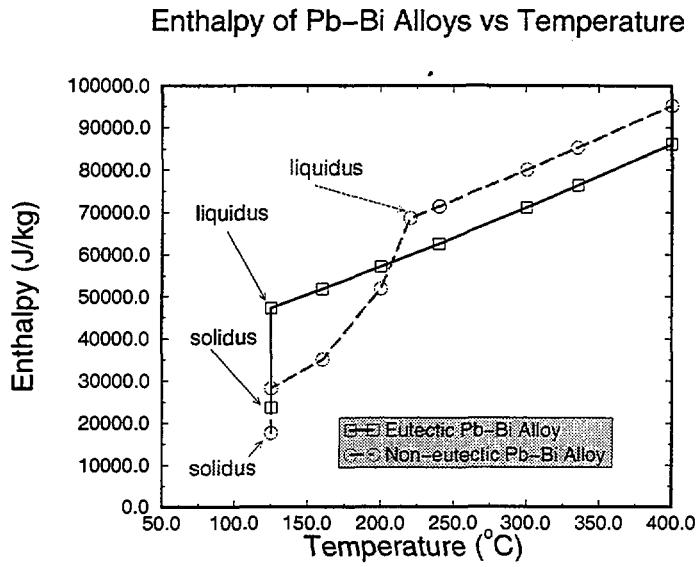

Figure 3.8: Variation of enthalpies of the eutectic and the non-eutectic Pb-Bi alloys with temperature

Figure 3.1 shows that when cooling at similar conditions, the non-eutectic drops (test series #6) begin their phase change process (i.e. enter the mushy zone) at a much greater temperature than the eutectic drops employed in test series #5. The fragmentation of a non-eutectic drop in test series #6 occurs only in the short time period when $240°C \geq T_m \geq T_{critical}$, within which the coolant temperature and cooling rate could exert some effect on the drop fragmentation. After the melt temperature $T_m < T_{critical}$, heat transfer has no more effect on the fragmentation process, and on the fragment size distribution. That is why the cumulative mass distribution, and the mass mean size, of the non-eutectic debris in test series #6 are not as sensitive to the coolant temperature as that of the eutectic debris in test series #5. Results similar to those shown in Figure 3.9 is obtained when the cumulative mass distributions produced from the eutectic drops in test series #8 are compared to that of the non-eutectic drops in test series #9.

Figure 3.10 compares the cumulative mass distributions resulting from fragmentation of the eutectic and the non-eutectic drops at equivalent superheats. It is seen from Figure 3.10 that even at lower (absolute) melt temperature, the eutectic drops (test series #7) appear to experience significantly deeper fragmentation (which is influenced by the coolant temperature) than the non-eutectic drops (test series #6). Results similar to those in figure 3.10 are obtained when the cumulative mass distributions obtained from eutectic drops in test series #5 are compared with those of the non-eutectic drops in test series #9. Again, the presence of the mushy zone may be responsible for this

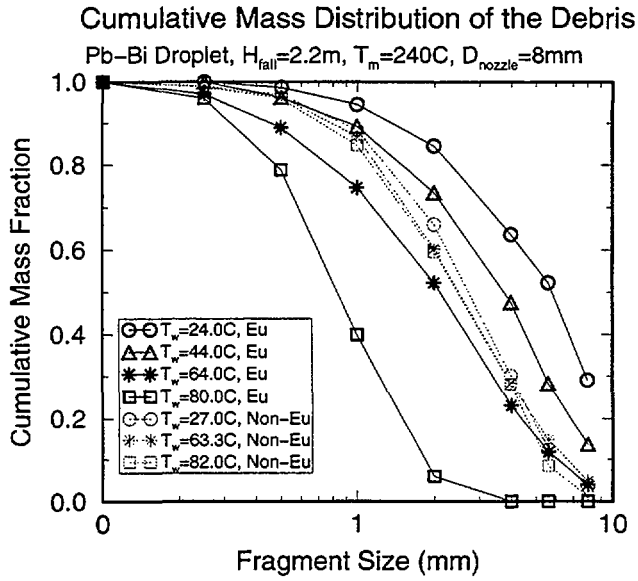

Figure 3.9: Effect of the melt composition (similar melt temperatures)

difference.

3.3 Stability Analysis of Drop Breakup with Crust Formation

3.3.1 Modeling objectives and assumptions

According to the experimental observation in section 2, different melt fragmentation regimes are governed by different physical phenomena. However, no matter what regime the melt fragmentation falls in, we believe that the drop breakup occurs because of the imbalance of forces acting on the drop. They are body, inertia, viscosity, surface tension and forces due to crust formation at the drop surface, as shown in figure 3.11. These forces can induce instability in the interface between the two liquids and perturbation can grow in time, and eventually, the drops break up.

In this section, a linear stability theory is employed to analyse the growth of perturbation on the drop surface. In order to simplify the model, we assume that the drop can

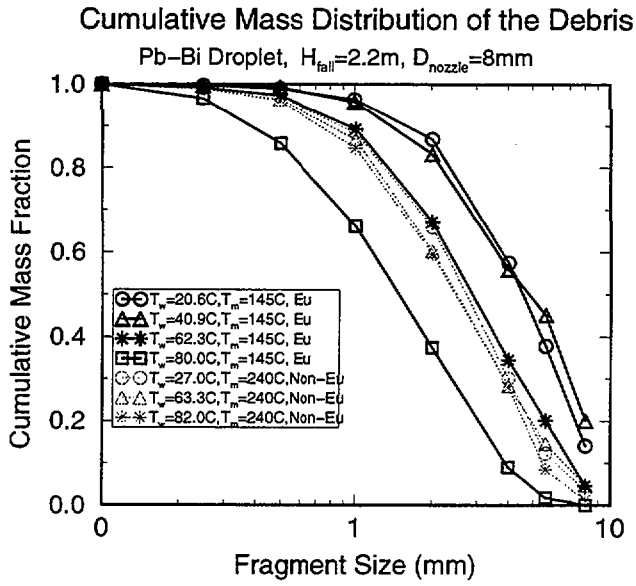

Figure 3.10: Effect of the melt composition (similar melt superheats)

be flattened out and looked upon as an infinitely flat interface, as shown in figure 3.12. Before we look at the instability between two relatively inviscid liquids with densities ρ_1, ρ_2, velocities U_1, U_2, temperatures T_1, T_2 surface tension σ and crust thickness δ, the following assumptions are made:

- The effect of viscosity, as a stabilizing influence, will be negligible in comparison with the stabilizing influence of the surface tension and crust, i.e. the Ohnesorge number $Oh = \mu_d/(\rho_d d_o \sigma)^{1/2}$ is assumed to be small.

- The crust layer at the interface is of zero thickness, inertia of the interface is negligible and the perturbations on the surface are small.

- Both upper and lower fluid are assumed to be incompressible liquids.

- Since the frozen layer is thin, the equation of bending theory of shells is employed and no edge effects are accounted for. Thermal stresses, due to bending and temperature gradient are neglected.

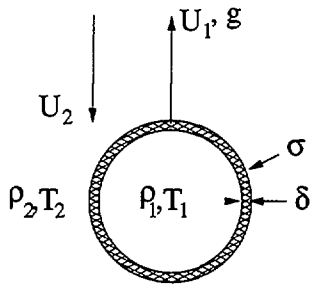

Figure 3.11: Drop with velocity U_1, acceleration g, density ρ_1, temperature T_1, surface tension σ and crust thickness δ interspersed in a liquid medium having velocity U_2, density ρ_2 and temperature T_2.

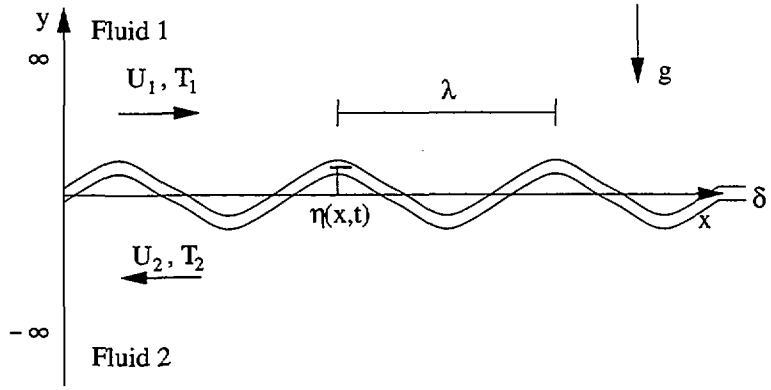

Figure 3.12: Waves of a frozen crust due to Kelvin Helmholtz and Rayleigh-Taylor instabilities.

3.3.2 Governing Equations

The continuity and Euler equations in two dimension for the upper and lower fluids can be written as:

$$\frac{\partial u}{\partial x} + \frac{\partial v}{\partial y} = 0 \tag{3.1}$$

$$\frac{\partial u}{\partial t} + U\frac{\partial u}{\partial x} = -\frac{1}{\rho}\frac{\partial P}{\partial x} + g_x \tag{3.2}$$

$$\frac{\partial v}{\partial t} + U\frac{\partial v}{\partial x} = -\frac{1}{\rho}\frac{\partial P}{\partial y} + g_y \tag{3.3}$$

If only the acceleration normal to the surface is considered, $g_x = 0$. Introducing the velocity potential ϕ at the interface, which can be written as a function of the displace-

ment $y = \eta(x,t)$ as [42]:

$$\frac{\partial \phi_1}{\partial y}(x,\eta,t) = \frac{\partial \eta}{\partial t} + U_1 \frac{\partial \eta}{\partial x} \tag{3.4}$$

$$\frac{\partial \phi_2}{\partial y}(x,\eta,t) = \frac{\partial \eta}{\partial t} + U_2 \frac{\partial \eta}{\partial x} \tag{3.5}$$

Considering the effects of the surface tension and the solidified crust, modified Laplace law can be expressed as [21]:

$$D\frac{\partial \eta^4}{\partial x^4} - 2\sigma \frac{\partial \eta^2}{\partial x^2} = P_2 - P_1 \tag{3.6}$$

where

$$D = \frac{E\delta^3}{12(1-\epsilon^2)} \tag{3.7}$$

The equations (3.4) to (3.6) have a solution of the following form [42]:

$$\phi_1 = -U_1 x - \phi_{01} \qquad \phi_2 = -U_2 x - \phi_{02} \tag{3.8}$$

and the pressure in the lower fluid can be expressed as [42]

$$P = \rho \frac{\partial \phi}{\partial t} + \rho U \frac{\partial \phi}{\partial x} - \rho g y \tag{3.9}$$

where the terms of second order or irrelevant to the present purpose are omitted. Additionally, the solution for ϕ must satisfy the following velocity potential for the continuity equation

$$\frac{\partial^2 \phi}{\partial x^2} + \frac{\partial^2 \phi}{\partial y^2} = 0 \tag{3.10}$$

and the boundary conditions

$$\frac{\partial \phi_1}{\partial x}(x,\infty,t) = 0 \qquad \frac{\partial \phi_2}{\partial x}(x,-\infty,t) = 0 \tag{3.11}$$

According to the specification of the equations (3.8) to (3.11), we apply the following solutions for the velocity potentials of both upper and lower fluids

$$\phi_1(x,y,t) = \phi_{01} \exp^{-ky} \exp^{i(nt-kx)} \quad \phi_2(x,y,t) = \phi_{02} \exp^{ky} \exp^{i(nt-kx)} \tag{3.12}$$

and displacement function as

$$\eta(x,t) = \eta_0 \exp^{i(nt-kx)} \tag{3.13}$$

where ϕ_{01} and ϕ_{02} are unknown constants. Putting equations (3.12) and (3.13) into equation (3.6) we get the following.

$$D\eta_0 k^4 + 2\sigma\eta_0 k^2 = \phi_{02}\rho_2 i(n + kU_2) - \phi_{01}\rho_1 i(n + kU_1) + \eta_0(\rho_1 - \rho_2)g \tag{3.14}$$

Inserting equations (3.12) and (3.13) into equations (3.4) and (3.5) gives,

$$\phi_{01}k = \eta_0 i(n + kU_1) \quad \phi_{02}k = \eta_0 i(n + kU_2) \tag{3.15}$$

Putting equation (3.15) into (3.14) gives the following equation for growth constant n.

$$(\rho_1 + \rho_2)n^2 + 2k(\rho_1 U_1 + \rho_2 U_2)n + Dk^5 + 2\sigma k^3 - (\rho_1 U_1^2 + \rho_2 U_2^2)k^2 - (\rho_1 - \rho_2)ak = 0 \tag{3.16}$$

The equation can then be solved easily for the growth constant n as,

$$n = \left[\frac{\rho_1\rho_2(U_1 - U_2)^2k^2}{(\rho_1 + \rho_2)^2} + \frac{(\rho_1 - \rho_2)ak}{\rho_1 + \rho_2} - \frac{Dk^5}{\rho_1 + \rho_2} - \frac{2\sigma k^3}{\rho_1 + \rho_2}\right]^{1/2} \tag{3.17}$$

where the wave number k can be replaced by the wavelength λ by inseting $k = 2\pi/\lambda$ into equation (3.17). We obtain

$$n = \left[\frac{(2\pi)^2\rho_1\rho_2(U_1 - U_2)^2}{\lambda^2(\rho_1 + \rho_2)^2} + \frac{2\pi(\rho_1 - \rho_2)g}{\lambda(\rho_1 + \rho_2)} - \frac{(2\pi D)^5}{\lambda^5(\rho_1 + \rho_2)} - \frac{2(2\pi)^3\sigma}{\lambda^3(\rho_1 + \rho_2)}\right]^{1/2} \tag{3.18}$$

On the right hand of this equation, the first term defines the destabilizing effect of the dynamic pressure drop, the second term may have destabilising effect if the acceleration is directed from the lighter phase towards the heavier phase or stabilising effect if the acceleration is towards the lighter phase from the heavier phase, the third and fourth terms stand for the stabilising effects of the solidified crust and the surface tension, respectively. The layer becomes unstable when the growth constant $n > 0$, which can be achieved when the first two terms are larger than the last two terms.

Next we will look into this case, by using the equation (3.17), when the destabilising dynamic pressure drop is large in comparison with the acceleration term, i.e. Kelvin-Helmholtz instability.

3.3.3 Kelvin-Helmholtz Instability

When the destabilising effect at the liquid interface is due to the dynamic pressure drop, a Kelvin-Helmholtz type of instability is generated. The surface tension or formation

of crust on the drop surface may prevent the growth of instability on the drop surface. In the current section we consider two cases, namely; (i) the fragmentation controlled regime when the surface tension term is dominant over the solidification term, and (ii) the freezing controlled regime when the solidification term is dominant over the surface tension force.

In the fragmentation controlled regime the dynamic pressure and the surface tension forces try to balance each other. An instability is obtained at the surface if $n > 0$ i.e., when the first term in equation (3.18) is larger than the fourth term

$$\frac{(2\pi)^2\rho_1\rho_2(U_1-U_2)^2}{\lambda^2(\rho_1+\rho_2)^2} > \frac{2(2\pi)^3\sigma}{\lambda^3(\rho_1+\rho_2)} \tag{3.19}$$

from which we can get

$$\lambda > \frac{4\pi\sigma(\rho_1+\rho_2)}{\rho_1\rho_2(U_1-U_2)^2} \tag{3.20}$$

Assuming that the maximum perturbation wavelength that can present a danger to the dro interface is of order $\lambda = d_o$, we get the following equation

$$\lambda_{max} = d_o > \frac{4\pi\sigma(\rho_1+\rho_2)}{\rho_1\rho_2(U_1-U_2)^2} \tag{3.21}$$

If $\rho_2 >> \rho_1$ then the following can be obtained,

$$We = \frac{d_o\rho_1(U_1-U_2)^2}{\sigma} > 4\pi \tag{3.22}$$

where We is the Weber number. This number is well known and used as a criteria for breakup of liquid drop in another fluid with no heat transfer, see e.g. Pilch [59] and Nigmatullin [53].

In the freezing controlled regime, solidification is dominant over the surface tension forces. When the first term in equation (3.18) is larger than the third term, the instability is generated at the drop interface

$$\frac{\rho_1\rho_2(U_1-U_2)^2k^2}{\lambda^2(\rho_1+\rho_2)^2} > \frac{(2\pi D)^5}{\lambda^5(\rho_1+\rho_2)} \tag{3.23}$$

from which we can get

$$\lambda > 2\pi\left[\frac{D(\rho_1+\rho_2)}{\rho_1\rho_2(U_1-U_2)^2}\right]^{1/3} \tag{3.24}$$

Again, assuming that the largest perturbations are of the order of the droplet diameter, we get

$$\lambda = d_o > 2\pi \left[\frac{D(\rho_1 + \rho_2)}{\rho_1 \rho_2 (U_1 - U_2)^2} \right] \tag{3.25}$$

If $\rho_2 >> \rho_1$, a modified Aeroelastic number Ae_* can be obtained

$$Ae_* = \frac{d_o^3 \rho_1 (U_1 - U_2)^2}{D} = \left(12(1-\epsilon^2) \frac{d_o}{\delta} \right)^3 Ae > Ae_{*,crit} \tag{3.26}$$

where Aeroelastic number is defined as $Ae = \rho_1 (U_1 - U_2)^2 / E$ and $Ae_{*,crit}$ is the critical Aeroelastic number i.e. above the critical Aeroelastic number breakup of drops can occur. Thus two distinct dimensionless numbers have been obtained. The well known Weber number (We) which is a characteristic breakup criterion for a drop in the fragmentation controlled regime. The second dimensionless number is the modified Aeroelastic number (Ae_*) which is a criterion for the breakup in the freezing controlled regime.

Furthermore the most unstable wavelength at the interface can be obtained by differentiating equation (3.18) with respect to λ, $dn/d\lambda = 0$. The most unstable wavelength λ_c, is obtained by isolating wavelength λ from the resulting equation, it gives

$$\lambda_c = \left[\sqrt[3]{R + \sqrt{Q^3 + R^2}} + \sqrt[3]{R - \sqrt{Q^3 + R^2}} + S \right]^{1/2} \tag{3.27}$$

$$Q = -\left(\frac{2\pi\sigma(\rho_1 + \rho_2)}{\rho_1 \rho_2 (U_1 - U_2)^2} \right)^2 \tag{3.28}$$

$$R = \frac{10(\pi)^3 D(\rho_1 + \rho_2)}{\rho_1 \rho_2 (U_1 - U_2)^2} - \left(\frac{2\pi\sigma(\rho_1 + \rho_2)}{\rho_1 \rho_2 (U_1 - U_2)^2} \right)^3 \tag{3.29}$$

$$S = \frac{1}{3} \left(\frac{2\pi\sigma(\rho_1 + \rho_2)}{\rho_1 \rho_2 (U_1 - U_2)^2} \right) \tag{3.30}$$

Now we look into the effect of crust thickness on the most unstable wavelength for the cerrobend-70 material. For the case that the relative velocity of the drop to that of the ambient is $U_d = U_1 - U_2 = 10$m/s and the ambient liquid is water, Figure 3.13 shows the effect of surface tension on the most unstable wavelength λ_c as a function of crust thickness δ. In general, if the crust thickness is small, the surface tension has dominant effect on the most unstable wavelength. When the surface tension is increased and the Weber number becomes lower the most unstable wavelength is shifted towards a higher value. In the case of large crust thickness the effect of surface tension becomes negligible and all the curves initially with different surface tension converge to a single curve. Figure 3.14 shows effect of the quantity $(\rho_1 + \rho_2)/(\rho_1 \rho_2 (U_1 - U_2)^2)$ on the most unstable wavelength. Similarly, the effect of crust is not significant when it is thin.

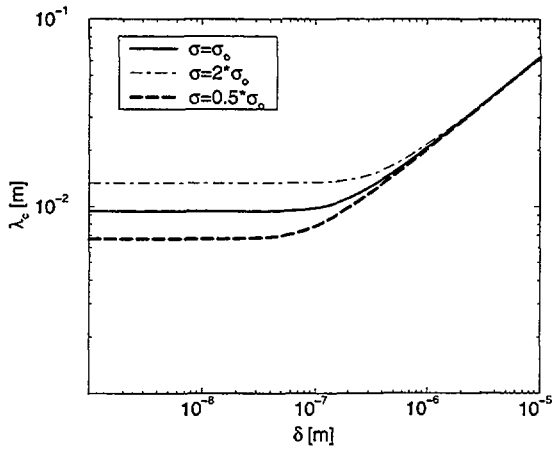

Figure 3.13: Effect of surface tension on the most unstable wavelength as a function of crust thickness

As the crust thickness grows, it begins to have significant effect on the most unstable wavelength. An increment in velocity or density seems to shift towards a lower most unstable wavelength.

3.3.4 Comparison with Experimental Results

The above-developed theory clearly reveals that the two-dimensional plain crust may break up when the modified Aeroelastic number (Ae_*) reaches its critical value of $(2\pi)^3$. As crust formation is of interest, the developed criterion is valid for drop when thin crust is formed before its breakup. However, the critical value of the modified Aeroelastic number (Ae_*) should be different from that for plain crust interface. In this section, an overall assessment of experimental data on drop fragmentation is performed by using the modified Aeroelastic number (Ae_*). First, however the evaluation of the crust thickness on the drop surface is presented.

Crust thickness estimation

As described above, the crust thickness of melt drop has a profound effect on the interface instability, and hence its fragmentation behaviour. It is very difficult to measure the crust thickness during the experiment. However, it is easy to estimate the time scales of

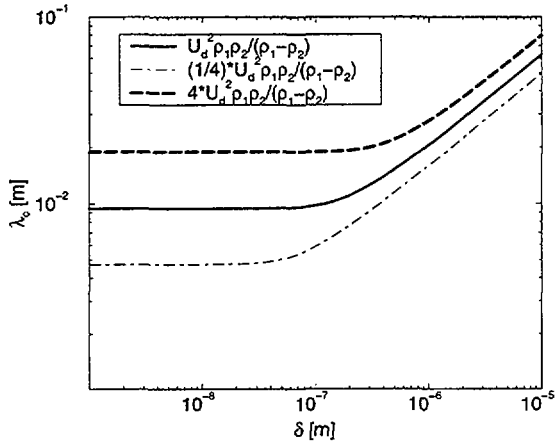

Figure 3.14: Effect of velocity and density on the most unstable wavelength as a function of crust thickness

fragmentation and solidification, which are importment parameters for the evaluation of the drop fragmentation behaviour.

In this paper the model proposed by Pilch and Erdman [60] for the characteristic time of drop fragmentation τ_f is employed, which is expressed as

$$\tau_f = t\frac{U_d \cdot (\rho_c/\rho_d)^{1/2}}{d_o} = f(We) \tag{3.31}$$

where the subscript d represents drop, D_o is the initial drop diameter. If one assumes that the originally stripped drop of cerrobend-70 has diameter of $d_o \approx 10$ mm and a velocity of $U_d \approx 3$ m/s then the characteristic times of breakup initiation, t_{ini}, primary breakup, t_{pri}, and total breakup, t_{tot}, as derived in [60] are 5, 17 and 37 ms respectively.

The timescale of solidification can be estimated by the time necessary to remove the melt superheat, $\Delta T_{sup} = T_j - T_{mp}$, and the melt heat of fusion, H_{fusion}, from a crust layer of thickness δ.

$$t_{sol} = t_{sup} + t_{fus} \tag{3.32}$$

where

$$t_{sup} = \frac{\rho_m \cdot C_{pm} \cdot \Delta T_{sup}\delta}{q"} \tag{3.33}$$

and

$$t_{fus} = \frac{\rho_m \cdot H_{fusion}\delta}{q"} \tag{3.34}$$

In the convective heat transfer regime, the heat flux is evaluated from [37].

$$q" = \frac{\kappa_c}{D_o}(2 + 0.6 \cdot Re^{0.5} \cdot Pr^{1/3})(T_d - T_c) \tag{3.35}$$

In nucleate boiling heat transfer regime, the Rosenhow correlation [33] is employed to estimate the heat flux

$$\frac{C_l(T_d - T_{sat})}{h_{fg}Pr_l} = C_{sf}\left[\frac{q/A}{\mu_l h_{fg}}\sqrt{\frac{\sigma}{g(\rho_l - \rho_v)}}\right]^{0.33} \tag{3.36}$$

Table 3.2 shows the solidification times for the cases with water temperatures of T_c = 5°C and T_c = 45°C and cerrobend-70 drop temperature of $T_d = 85°C$. The thickness of the crust layer [1] is varied between 10μm and 50μm. Such a calculation reveals that for a 20μm-crust layer in cold water, the characteristic solidification time may be less than that of primary breakup. This supports the observation from the experiments that particle debris sizes were smaller under cold water conditions.

Table 3.2: Characteristic times of solidification to form a given crust thickness for $T_d = 85°C$.

Crust thickness	t_{sol} (ms)	
δ (μm)	T_c = 5°C	T_c = 45°C
10	4.6	9.1
20	9.3	18.1
30	13.9	27.2
40	18.5	36.3
50	23.2	45.3

Assessment of drop fragmentation by the modified Aeroelastic number (Ae_*)

The experimental data obtained in present paper, as well as the experimental data obtained by Yang and Bankoff [78] are used here. In the experiments by Yang and Bankoff a shock wave was generated in a shock tube and directed over a Cerrobend-70 drop which either fragmented or deformed the fluid drop depending on the experimental conditions. In their work, the crust thickness was then calculated by thermal balance

[1] The value of δ which will prohibit subsequent drop fragmentation will of course depend on melt physical properties and the flow conditions.

between the drop and the surrounding coolant media. Those tests are thus somewhat different from our test setup. Instead of accelerating the drop as our experiments, the surrounding was accelerated over the drop surface.

Figure 3.15 shows the modified Aeroelastic number as a function of the dimensionless crust thickness δ/d_o (where d_o is the initial drop diameter) for the data of Cerrobend-70 drop, which include both our experimental data and the experimental data obtained by Yang and Bankoff [78]. It can be seen from figure 3.15 that there

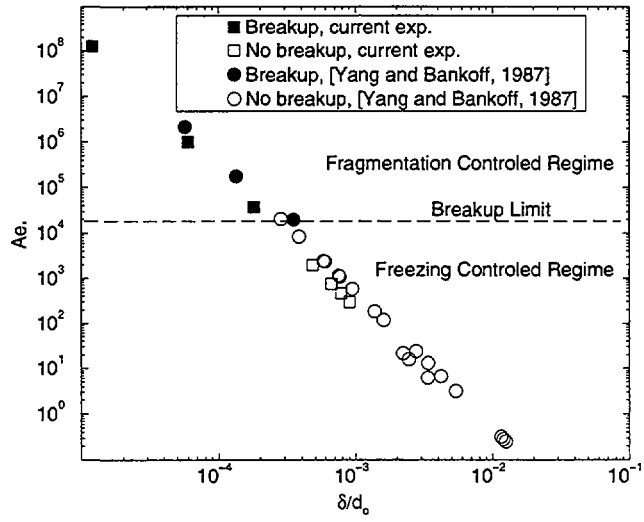

Figure 3.15: Modified Aeroelastic number (Ae_*) as a function of the dimensionless crust thickness for Cerrobend-70 experimental data obtained by the authors and by [78].

is a very clear interface between breakup and no-breakup regimes for both experiments, the breakup of the drop occurs if the modified Aeroelastic number is above $Ae_* \simeq 2*10^4$, which may be regarded as the critical Aeroelastic number for drop fragmentation. Above this critical Aeroelastic number, all drops fragmented, we can call this regime as fragmentation controlled regime. Below this critical Aeroelastic number, the crust thickness is large enough to prevent the drop breakup, the freezing controlled regime is observed. More importantly, for the current experiments, when the modified Aeroelastic number reaches its critical value, the dimensionless crust thickness δ/d_o is approximately $\delta/d_o \sim 3*10^{-4}$, which seems to be about the same as in the experimental data obtained by Yang and Bankoff [78]. In their evaluation of the crust thickness, a different method was employed, however, there is hardly any difference in the drop

crust thickness evaluation between these two methods.

Figure 3.16 shows the modified Aeroelastic number as a function of dimensionless crust thickness for the experiments with Pb-Bi drops. As it can be seen that the breakup

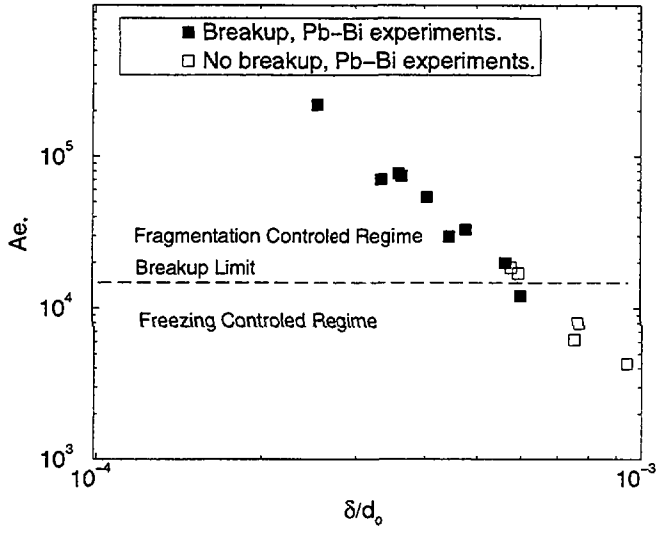

Figure 3.16: Modified Aeroelastic number (Ae_*) as a function of the dimensionless crust thickness for the Pb-Bi experimental data.

limit is observed and hence the two regimes; the fragmentation controlled regime and the freezing controlled regime are again observed. Moreover, the critical modified Aeroelastic number is about $2*10^4$, which is almost the same as that for the Cerrobend-70 data. However, the dimensionless crust thickness is found to be the little higher value of $\delta/d_o \sim 5 * 10^{-4}$, which results from the different physical properties of these two materials, which affect the heat transfer inside the drop.

It may be concluded that the modified Aeroelastic number can be used to evaluate the breakup behaviour of a drop with crust formation on its surface. According to above-analysed results, the critical modified Aeroelastic number is about $1.7 * 10^4$, above which, the drop falls into fragmentation controlled regime, and below which no breakup of drop occurs. The value of critical modified Aeroelastic number is found to be independent of the drop material and its physical properties.

More importantly, it is found that the modified Aeroelastic number can be employed to evaluate the average diameters of the fragmented particles. If the modified

Aeroelastic number is higher than the critical modified Aeroelastic number of $1.7*10^4$, the drops only deform and little stripping is observed from the surface, in this case $d_{mean}/d_o \sim 1$, i.e. the mean size should be of the order of the initial drop size. When the modified Aeroelastic number is increased $1.7*10^4 < Ae_* < 2.5*10^5$, the drop will fall into the fragmentation controlled regime and hence break up. By plotting the data obtained in the experiments with Pb-Bi drops, it is found that the dimensionless mean diameter of the fragmented particles d_{mean}/d_o are obviously related to the modified Aeroelastic number Ae_*. This dependence can be expressed as:

$$\frac{d_{mean}}{d_o} = A\exp(B(Ae_*) \tag{3.37}$$

where $A = 0.4$ and $B = -9.7 * 10^{-6}$ are constants obtained by fitting the experimental data with Pb-Bi drop data. Figure 3.17 shows the normalised drop diameter as a function of the modified Aeroelastic number for the Pb-Bi data. As it can be seen from this correlation, the drop with larger modified Aeroelastic number always leads to the formation of the smaller fragmented particle. However, more experimental data are required to validate this correlation.

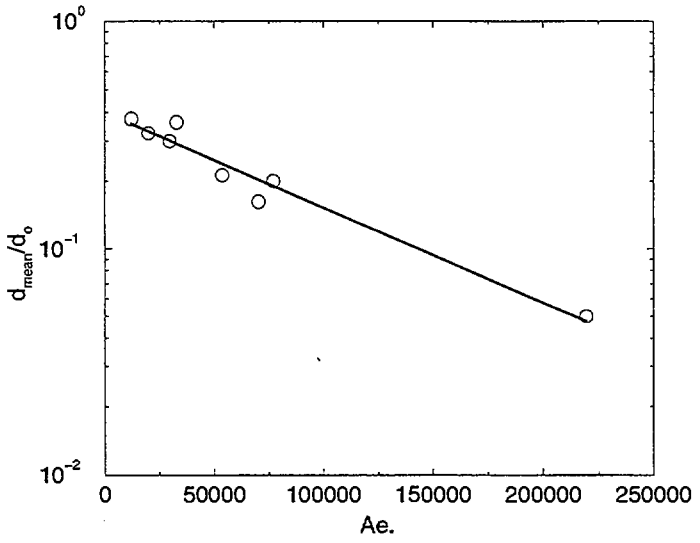

Figure 3.17: Normalized drop diameter d_{mean}/d_o as a function of Ae_* for the the Pb-Bi experimental data

3.4 Concluding Remarks

Experiments on drop fragmentation were performed for different melt materials and with different physical parameters. It is found that coolant temperature has a significant influence on the drop fragmentation behaviour for subcooled conditions. During the drop coolant interaction processes, the solidification and the fragmentation processes and their time scales compete with each other. The competition results leads to the fragmentation-controlled regime and the freezing-controlled regime. The melt superheat greatly affects the characteristic time for solidification, and thus strongly affects the deepness of the fragmentation process.

An instability analysis on the crust breakup has been performed. A modified dimensionless Aeroelastic number Ae_* is obtained as a criterion for breakup of a planar crust. It is found that the modified Aeroelastic number can be employed to evaluate the drop breakup behavior in a liquid pool with solidification on its surface. The critical modified Aeroelastic number is about $2 * 10^4$. Above this critical modified Aeroelastic number the drops fall into the fragmentation controlled regime and the drop will break up even though the crust is formed at its surface. Below the critical modified Aeroelastic number the freezing controlled regime is obtained and no breakup of the drops will occur. A correlation for the ratio of the fragmented mean drop size to the initial drop size as a function of the modified Aeroelastic number is found. It is found that the drop diameter varies exponentially with the modified Aeroelastic number. However, more experimental data are required to validate the developed criterion and correlation, for which the properties of drop and other thermal hydraulic parameters should be tested.

Chapter 4

Conclusions

In this chapter, main results of the thesis are summarised. The main objective of the thesis is to improve understanding of the breakup process of melt jets and drops under MFCI conditions.

The breakup of the melt jet under MFCI conditions was investigated in Chapter 2. Low temperature jet breakup experiments were conducted to investigate the impact of thermal-hydraulic conditions upon the breakup behaviour and the particle debris bed characterization for the interaction of a melt jet in water. An alloy with 70°C melting point was used as jet liquid in non-boiling mode experiments where coolant conditions were varied to provide insight into jet fragmentation with and without melt freezing. Coolant temperature was found to significantly affect both the size and the shape of particles stripped/fragmented from the melt jet. Coolant tank void fractions (air) up to 20% did not reveal any substantial impact on the average particle size or size distribution. The findings were presented in terms of the competing time scales related to the solidification process and to sequential particle fragmentation. High temperature experiments were performed using CaO-B_2O_3, MnO_2-TiO_2 and WO_3-CaO as jet material. The coolant temperature was found to significantly influence the characteristics of debris fragments produced from the jet breakup. It was found that at low subcooling the fragments are relatively large and irregular compared to smaller particles produced at high subcooling. The melt jet density has considerable effect on the fragment size produced. As the melt density increases the fragment size becomes smaller. The mass mean size of the debris changes proportionally to the root of the melt to coolant density ratio. This is in good agreement with theoretical stability analysis. The melt superheat was found to have little effect on the debris particle size distribution produced during the melt jet fragmentation. The impingement velocity of the jet was found to have a

significant impact on the fragmentation process. At lower jet velocity the melt agglomerates and forms a cake of large size debris. When the jet velocity is increased more complete fragmentation is obtained. Examination of four different statistical models for particle size distribution indicates that the sequential fragmentation theory of Brown [8], which results in a Gamma type distribution, provides the best fit the debris distribution data. The fractal dimension varies between two and three for the experimental data analysed. There is no clear correlation between the experimental conditions and the fractal dimension.

In chapter 2, the MELT-3D method is applied for simulation of continuous jet fragmentation. Parametric investigation of coolant properties and jet/coolant velocities demonstrated the model capabilities to analyse the complex processes of multiphase mixing. It was found that the method is computationally robust, inexpensive and does not encounter problems of excessive numerical diffusion and oscillations, which usually result from the Eulerian representation of the melt phase. Furthermore, numerical simulations of Kelvin-Helmholtz instability on an interface between two density-matched fluids were performed, the effects of surface tension, initial perturbation amplitude and viscosity were investigated. Simulation results show that the interfacial structure changes dramatically as the Weber number We varies. The lower the Weber number, the smaller the wave growth rate is observed and the smoother the interface appears. If the Weber number is low enough and the initial perturbation amplitude is small, the present numerical simulation on the interface evolution agrees qualitatively with the predictions of the linear instability theory. As Weber number increases, substantial deviations from the linear theory are observed. The presence of viscosity reduces the growth of the initial wave. Nonlinearity introduced by large initial perturbation appears to damp the small-scale instabilities.

Chapter 3 is dedicated to the breakup of drops with solidification. Results from experimental investigation on drop breakup using Pb-Bi alloys at both eutectic and non-eutectic compositions were presented. Coolant temperature was found to have significant impact on the droplet fragmentation behaviour for subcooled conditions. Typically, the droplet fragmentation can be roughly categorized in two regimes: the fragmentation-controlled regime, and the freezing-controlled regime. The solidification and the fragmentation processes and their time scales compete with each other. The melt superheat greatly affects the characteristic time for solidification, and thus strongly affects the deepness of the fragmentation process. The fusion heat of the eutectic melt contributes significantly to the solidification time scale, and thereby enabling the eutectic melt drop to feature deeper fragmentation. The presence of the mushy zone during the phase change of the non-eutectic melts significantly prevents these melt drops from completing the deformation and fragmentation process, especially when the melt superheat is small. Compared to the effect of the melt physical properties in the mushy zone (e.g. viscosity, surface tension), the fusion heat of the non-

eutectic melt plays a relatively smaller role in the fragmentation process. An instability analysis on the crust breakup was performed. A modified dimensionless Aeroelastic number Ae_* is obtained as a criterion for breakup of a planar crust. It is found that the modified Aeroelastic number can be employed to evaluate the drop breakup behavior in a coolant pool with the effect of solidification on its surface. The critical modified Aeroelastic number is about $2 * 10^4$. Above this critical modified Aeroelastic number the drops fall into the fragmentation controlled regime and a drop will break up even though the crust is formed at its surface. Below the critical modified Aeroelastic number the freezing controlled regime is obtained and no breakup of the drops occurs. A correlation for the ratio of the mean drop size of the fragmented drops to the initial drop size as a function of the modified Aeroelastic number is found. It is found that the drop diameter varies exponentially with the modified Aeroelastic number. However, more experimental data is required to validate the developed criterion and correlation, for which the properties of drop and other thermal hydraulic parameters should be tested.

Bibliography

[1] Adalsteinsson, D., and Sethian, J.A., 1995, A Level Set Approach to a Unified Model for Etching, Deposition, and Lithography I: Algorithms and Two-Dimensional Simulations, *J. of Comput. Phys.*, v.120, pp.128-144.

[2] Angelini, S., Yuen, W.W., and Theofanous, T.G., 1995, Premixing-Related Behaviour of Steam Explosions, *Nuclear Engineering and Design*, v.155, pp.115-157.

[3] Annunziato, A. and Addabbo, C., "COMETA (Core Melt Thermal-hydraulic Analysis)- A Computer Code for Melt Quenching Analysis", Proceedings of the International Conference on New Trends in Nuclear System Thermohydraulics, Pisa, Italy, 1994.

[4] Berthoud, G., and Valette, M., 1994, Development of a Multidimensional Model for the Premixing Phase of a Fuel-Coolant Interaction, *Nuclear Engineering and Design*, v.149, pp.409-418.

[5] Berthoud G., 1996, "Progress Made in the Area of Molten Fuel Coolant Interaction", *Proceeding of the FISA 95 Symposium on EU Research on Severe Accidents*, pp.119-139, 20-22 November 1995, Luxembourg; also "Molten Fuel-Coolant Interactions" in EUR-17126 EN, Luxembourg, 1996.

[6] Berthoud, G., Oulmann, T. and Valette, M., Corium-Water Interaction Studies in France, *Proceeding of the FISA 95 Symposium on EU Research on Severe Accidents*, Luxembourg, 1996.

[7] Bilbao, R.M., Chu, C.C., Corradini, M.L., Huhtinieme, I., Murphy, S., Nilsuwankosit, J.T., "TEXAS Code Manual: A One Dimensional Transient Model for Fuel-Coolant Interaction Analysis", University of Wiscounsin, 1996.

[8] Brown, W.K., "A Theory of Sequential Fragmentation and Its Astronomical Applications", Journal of Astrophysics, Vol 10 (1989), pp. 89-112.

[9] Bui, V.A., Dinh, T.N., and Sehgal, B.R., *Numerical Simulation of Surface Instability Phenomena Associated with Fuel-Coolant Interaction*, Proceedings of the Eighth

International Topical Meeting on "Nuclear Reactor Thermal Hydraulics, NURETH-8", Kyoto, Japan, September 1997, Vol.2, pp.639-646.

[10] Bui, V.A., Dinh, T.N., and Sehgal, B.R., "Analysis of Liquid Jet Instability: Effect of Physical Properties", SKI Report 98:21, Appendix 11, SKI, 1998.

[11] Bürger M, S.H. Cho, Berg, E.v., and Schatz, A., "Breakup of Melt Jets as Precondition for Premixing: Modeling and Experimental Verification". *Nuclear Engineering and Design*, Vol.155 (1995), pp.215-251.

[12] Chandrasekhar, S. Hydrodynamic and Hydromagnetic Stability. *Oxford at the Clarendon Press*, 1961.

[13] Cheiger, N. and Reitz, R.D., Regimes of Jet Breakup and Breakup Mechanism (Physical Aspects) In *Recent Advances in Spray Combustion: Spray Automization and Drop Burning Phenomena*, Progress in Astronautics and Aeronautics, ed. K.K. Kuo, **Vol. 171**, pp. 109-135, (1996).

[14] Chen, X., Yuen, W.W. and Theofanous, T.G., "On The Constitutive Description of Microinteractions Concept in Steam Explosions", Proceedings of the Seventh International Topical Meeting on Nuclear Reactor Thermal Hydraulics NURETH-7, New York, USA, 1995, NUREG/CP-0142.

[15] Chu, C.C, Sienicki, J.J., Spencer, B.W., Frid, W., and Löwenhielm, G., 1995, "Ex-vessel Melt-Coolant Interactions in Deep Water Pool: Studies and Accident Management for Swedish BWRs." *Nuclear Engineering and Design,* Vol.155 (1995), pp.159-213.

[16] Corradini, M.L., Kim, B.J. and Oh, M.D., "Vapor Explosions in Light Water Reactors: A Review of Theory and Modeling", *Progress in Nuclear Energy*, Vol. 22, 1988, pp. 1-117.

[17] Davis, F.J., and Young, M.F., 1994, Integrated Fuel-Coolant Interaction (IFCI 6.0) Code User's Manual, NUREG/CR-6211, SAND94-0406, April 1994, Sandia National Laboratories, Albuquerque, NM87185.

[18] M.K. Denham, A.P. Tyler and D.F. Fletcher, "Experiments on the Mixing of Molten Uranium Dioxide with Water and Initial Comparision with CHYMES Code Calculations", ANS Proc. of 5th International Topical Meeting on Reactor Thermal Hydraulics, 21-24 September, Salt Lake City, US, 1992, pp. 1667-1675.

[19] Dinh, A.T., Dinh, T.N., Nourgaliev, R.R., and Sehgal, B.R., "Simulation of Melt Coolant Interactions in a Steam Explosion", CD-ROM Proceedings of the Third International Conference on Multiphase Flow, ICMF'98, June 8-12, 1998, Lyon, France.

[20] Dinh, T.N., Bui, V.A., Nourgaliev, R.R, Green, J.A. and Sehgal, B.R., "Experimental and Analytical Studies of Melt Jet-Coolant Interactions: A Synthesis", Proceedings of 2nd OECD/CSNI Specialist Meeting on Fuel-Coolant Interactions, JEARI-Tokay, Japan, May 19-21, 1997.

[21] Epstein, M., Stability of Submerged Frozen Crust, Journal of Heat Transfer, **99**, 1977, pp. 527-532.

[22] Epstein, M. and Fauske, H.K., "Steam Film Instability and the Mixing of Core-Melt Jets and Water." *ANS Proceedings of the 1985 National Heat Transfer Conference*, Denver, Colorado, USA, 1985, pp.277-284.

[23] Fletcher, D.F., "The Particle Size Distribution of Solidified Melt Debris from Molten Fuel-Coolant Interaction Experiments", Nuclear Engineering and Design, Vol 105 (1988), pp. 313-319.

[24] Fletcher D.F., and Denham, M.K., 1995, Validation of the CHYMES Mixing Model, *Nuclear Engineering and Design*, v.155, pp.85-96.

[25] Gelfand, B.E., "Droplet Breakup Phenomena in Flows with Velocity Lag", Progress in Energy and Combustion Science, Vol 22 (1996), pp. 201-265.

[26] Gingsberg, T., "Liquid Jet Breakup Characterization with Application to Melt-Water Mixing", Proc. of Intern. ANS/ENS Topical Meeting on Thermal Reactor Safety, San Diego, CA, II.4, 1986, pp. 1-18.

[27] Grigull, U., Straub, J., and Schiebener, P., "Steam Tables in SI-Units", Springer-Verlag, Berlin, 1984.

[28] Hall, R.W., and Fletcher D.F., 1995, Validation of CHYMES: Simulant Studies, *Nuclear Engineering and Design*, v.155, pp.97-114.

[29] Haraldsson, H.Ó, Li, H.X., Dinh, T.N., Green, J.A. and Sehgal, B.R., "Hydrodynamic Fragmentation of Molten Metal Jet in Water: Effect of melt solidification and coolant voiding", Twelfth Proceedings of Nuclear Thermal Hydraulics, ANS (1997), pp. 125-134.

[30] Haraldsson, H.Ó, Li, H.X., Dinh, T.N., Green, J.A. and Sehgal, B.R., "Hydrodynamic Fragmentation of Molten Metal Jet in Water: Effect of melt solidification and coolant voiding", RIT/NPS Technical report MFCI-97-JF1, May 1997.

[31] Haraldsson, HÓ. and Sehgal, B.R., "Particle Size Distribution in Molten Fuel-Coolant Interactions and Parameters of the Sequential Fragmentation Theory", CD-Rom Proc. of the 3rd Int. Conf. On Multiphase Flow, ICMF'98, Lyon, France, June 8-12, 1998.

[32] Hirt, C.W. and Nichols, B.D., "Volume of Fluid (VOF) Method for the Dynamics of Free Boundaries", Journal of Computational Physics, Vol 39., pp. 201-225, 1981.

[33] J.P. Holman, "Heat Transfer", McGraw Hill, 1989.

[34] Hou, T.Y., Lowengrub, J.S. and Shelley, M.J., *The Long-Time Motion of Vortex Sheets with Surface Tension* Phys. Fluids, n9, pp. 1933, 1997.

[35] Hsiang, L.P. and Faeth, G.M., "Drop deformation and Breakup Duo to Shock Wave and Steady Disturbances", Int. J. Multiphase Flow, Vol.21, No.4, pp.545-560, 1995.

[36] Huhtiniemi, I., Hohmann, H., Magallon, D., "FCI Experiments in the Corium/Water System", Proceedings of the 7th International Meeting on Nuclear Reactor Thermal-Hydraulics, NURETH-7, Saratoga Springs, New York. September 10-15, pp.1712-1727, 1995.

[37] Incropera, F.P. and DeWitt, D.P., "Fundamentals of Heat and Mass Transfer", John Wiley & Sons, 1990.

[38] Irani, R.R. and Callis, C.F., "Particle Size: Measurements, Interpretation and Applications", John Wiley and Sons, New York, 1963.

[39] Kim, D.S., IKE Bericht 2-68, Stuttgart University, 1985.

[40] Kolev, N.I., 1993, The Code IVA3 for Modeling of Transient Three-Phase Flows in Complicated 3-D Geometry, *Kerntechnok* 58, 147-15.

[41] Kolev, N.I., 1996, Three Fluid Modeling with Dynamic Fragmentation and Coalescence: Fiction of Daily Practice?, *OECD/CSNI Workshop on Transient Thermal-Hydraulic and Neutronic Codes Requirements*, Annapolis, Md, USA, 5-8 November 1996.

[42] Lamb, Sir H., Hydrodynamics, sixth edition, Dover, 1932.

[43] Levich,V.G., Physicochemical Hydrodynamics. *Prentice-Hall*, Englewood Cliffs, NJ, 1962.

[44] Li, H.X., Haraldsson, HÓ., Dinh, T.N., Green, J.A. and Sehgal, B.R., "Fragmentation Behavior of Melt Drops in Coolant: Effects of Melt Drop Solidification", CD-Rom Proc. of the 3rd Int. Conf. On Multiphase Flow, ICMF'98, Lyon, France, June 8-12, 1998.

[45] Lin, S.P. and Reitz, R.D., Drop and Spray Formation from a Liquid Jet. *Annual review of Fluid Mechanics*, **30**, pp. 85-105, (1998).

[46] Lupis, C.H.P., "Chemical Thermodynamics of Materials", Elsevier Science Publishing Co., Inc., New York, NY,1983.

[47] Magallon D., Will H., Turland B.D., Annunziato A., Dobson G.P., Horváth G.L., Lummer M., Väth L., Valette M., and Valisi M., "High Temperature Melt/Water Mixing: Results and Calculations of FARO, PREMIX and MIXA Experiments", *Proceeding of the FISA 95 Symposium on EU Research on Severe Accidents*, pp.140-164, 20-22 November 1995, Luxembourg.

[48] Magallon, D., Huhtiniemi, I. and Hohmann, H., "In-Vessel Loads Resulting From Molten Coolant/Structure Interactions", Proceedings of Service Experience, Structural Integrity Severe Accidents, and Erosion in Nuclear and Fossil Plants, ASME, PVP-Vol. 303 (1995).

[49] Magallon, D., Huhtiniemi, I. and Hohmann, H., "An Overview of FARO and KROTOS Test Results", Proceedings of PSA '96, Utah, USA.

[50] Magallon, D., Huhtiniemi, I. and Hohmann, H., "Lessons Learnt from FARO/TERMOS Corium Melt Quenching Experiments", Nuclear engineering and Design, Vol. 189, pp. 223-238, 1999.

[51] Melikhov, O.I., and Melikhov, V.I., "Investigation of Processes of Melt-Water Interactions during Nuclear Reactor Severe Accidents", Preprint EREC, Electrogorsk, Moscow, 1993 (in Russian).

[52] Meyer, L., The Interaction of a Falling Mass of Hot Spheres with Water, ANS Proceedings of 1996 National Heat Transfer Conference, August 3-6 1996, pp. 105-116.

[53] Nigmatulin, R.I., Dynamics of Multiphase Media, Hemisphere Publication Company, 1990.

[54] Nourgaliev, R.R., Dinh, T.N. and Sehgal, B.R., "Simulation of Multiphase Mixing by a Particle Transport Model", CD-ROM Proceedings of the 5th International Conference on Nuclear Engineering, Nice, France, May 26-30, 1997.

[55] R.R. Nourgaliev, T.N. Dinh, A.T. Dinh, H.Ó. Haraldsson and B.R. Sehgal, "The Multiphase Eulerian-Lagrangian Transport (MELT-3D) Approach for Modeling of Multiphase Mixing in Fragmentation Processes", International Journal of Multiphase Flow. (submitted)

[56] S. Osher and J.A. Sethian, "Fronts Propagating with Curvature-Dependent Speed: Algorithms Based on Hamilton-Jacobi Formulations". J. Comp. Physics **79**, pp.12-49, 1988.

[57] Okkonen, T.J., and Sehgal, B.R., Experiments on Melt Droplets Falling into a Water Pool, Proceedings of the 2nd OECD/CSNI Specialist Meeting on Fuel-Coolant Interactions, JAERI-Tokai, Japan, May 19-21, 1997.

[58] Patel, P.D. and Theofanous, T.G., "Hydrodynamic Fragmentation of Drops", Journal of Fluid Mechanics, Vol.103, 1981, pp.207-223.

[59] Pilch, M.M., "Acceleration-Induced Fragmentation of Liquid Drops", NUREG/CR-2247 R7, 1981, 263p.

[60] Pilch, M.M. and Erdman, C.A., "Use of Breakup Time Data and Velocity History Data to Predict the Maximum Size of Stable Fragments for Acceleration-Induced Breakup of a Liquid Drop". Int. J. Multiphase Flow, Vol.13, No.6, pp. 741-757, 1987.

[61] Platau, J., "Statique Experimentale et Theorique des Liquids Soumie aux Seules Forces Molecularie", Vol. 1,2, Paris: Cauthier Villars, 1873.

[62] Rayleigh, Lord On the Capilary Phenomena of Jets.*Proc. Royal Soc. London*, 1879.

[63] Sehgal, B.R., Bui, V.A., and Dinh, T.N., *Accurate Numerical Simulation of Interface Phenomena in Two Phase Flow* 2nd International Conference on Heat Transfer and Transport Phenomena in Multiphase Systems, Kielce, Poland, May 18-22, 1999.

[64] Sehgal, B.R., "Accomplishments and Challenges of the Severe Accident Research", Ninth International Conference on Nuclear Reactor Thermal Hydraulics, San Francisco, CA, 1999.

[65] Speis, T. P., and Basu, S., 1997, Fuel Coolant Interaction (FCI) Phenomena in Reactor Safety: Current Understanding and Future Research Needs, *Proceedings of the OECD/CSNI/NEA Specialist Meeting on Fuel Coolant Interactions*, Tokai-Mura, Japan, May 1997.

[66] Taylor, G.I. Generation of ripples by wind blowing over viscous fluids. In *The Scientific Papers of G.I Taylor*, ed. G.K. Batchelor, Cambridge University Press, 3 pp. 244-55

[67] Theofanous, T.G., Yuen, W.W., and Angelini, S., "The Internal Dynamic Structures of a Class of Transient Dispersed Flows with Phase Change", CD-ROM Proceedings of the Third International Conference on Multiphase Flow, ICMF'98, June 8-12, 1998, Lyon, France.

[68] Theofanous, T.G., and Yuen, W.W., 1995, The Probability of Alpha-Mode Containment Failure Updated, *Nuclear Engineering and Design*, v.155, pp.459-473.

[69] Theofanous, T.G., et al., 1996, Lower Head Integrity under In-Vessel Steam Explosions Loads, *DOE/ID-10541*, (June 1996).

[70] Tomotika, S., On the Instability of a Cylindrical Thread of a Viscous Liquid Surrounded by Another Viscous Liquid. *Proc. Royal Soc. A*, **150**, pp. 322-327, (1935)

[71] Turland, B.D. and Dobson, G.P., 1996, "Molten Fuel Coolant Interactions: A State of the Art Report", EUR 16874 EN, Luxembourg, 1996.

[72] Turland, B.D., Fletcher, D.F., Hodges, K.I., and Attwood, G.J, 1993, Quantification of the Probability of Containment Failure Caused by an In-Vessel Steam Explosion for the Sizewell B PWR, *CSNI Specialists Meeting on Fuel-Coolant Interactions*, Santa Barbara, CA.

[73] Univerdi, S.O. and Tryggvason, G., "A Front-tracking Method for Viscous, Incompressible, Multi-fluid Flows, Journal of Computational Physics, Vol. 100, pp. 25-37, 1992.

[74] Weber, C.Z. , Zum Zerfall eines Flussigkeitsstrahles *Math. Mech*, **11**, pp. 136-154, (1931)

[75] Weibull, W., "A statistical Distribution Function of Wide Applicability", Journal of Applied Mechanics", 18 (1951), pp. 193-197.

[76] Wennerstrom, H., "Experimental Investigations of the Minimum Film Boiling Temperature on a Vertical Surface and the Effect of Surfactants on Film Boiling for Discrete Drops of Water on a horizontal Plate", Licentiate Thesis, Department of Energy of Technology, Division of Nuclear Reactor Engineering, Royal Institute of Technology, Stockholm, Sweden, October, 1996.

[77] Yang, H.Q., "Asymmetric Instability of a Liquid Jet". *J. Phys. Fluids A*, **4**(4), pp.681-688, 1992.

[78] Yang, J.W. and Bankoff, S.G., Solidification Effects on the Fragmentation of Molten Metal Drops Behind a Pressure Shock Wave, Journal of Heat Transfer, **109**, 1987, pp. 226-230.

[79] Young, M.F., "Integrated Fule-Coolant Interaction (IFCI-7.0) Code User's Manual", Sandia Report, SAND99-0999, May, 1999.

[80] Yuen, W.W., Chen, X.,and Theofanous, T.G., "On the Fundamental Micro-interactions that Support the Propagation of a Steam Explosion", Nuclear Engineering and Design, Vol.146, pp.133-146, 1994.